

Influences on the rotated structure of diiron dithiolate complexes: electronic asymmetry vs. secondary coordination sphere interaction†

Yu-Chiao Liu,^a Ling-Kuang Tu,^a Tao-Hung Yen,^a Gene-Hsiang Lee^b and Ming-Hsi Chiang^{*a}

Received 5th October 2010, Accepted 8th December 2010

DOI: 10.1039/c0dt01332c

In the pursuit of a “rotated” structure, and exploration of the influence of the aza nitrogen lone pair, the Fe^IFe^I model complexes wherein two Fe(CO)_{3-x}P_x moieties are significantly twisted from the ideal configuration (torsion angle >30°) are reported. [Fe₂(μ-S(CH₂)₂NⁱPr(X)(CH₂)₂S)(CO)₄(κ²-dppe)]₂²⁺ (X = H, **4**; Me, **5**) prepared from protonation and methylation, respectively, of [Fe₂(μ-S(CH₂)₂NⁱPr(CH₂)₂S)(CO)₄(κ²-dppe)]₂, **1**, possess Φ angles of 34.1 and 35.4° (av.), respectively. Such dramatic twist is attributed to asymmetric substitution within the Fe₂ unit in which a dppe ligand is coordinated to one Fe site in the κ²-mode. In the presence of the N⋯C(CO_{ap}) interaction, the torsion angle is decreased to 10.8°, suggesting availability of lone pairs of the aza nitrogen sites within **1** is in control of the twist. Backbones of the bridging diphosphine ligands also affect distortion. For a shorter ligand, the more compact structure of [Fe₂(μ-S(CH₂)₂NⁱPr(CH₂)₂S)(μ-dppm)(CO)₄]₂, **7**, is formed. Dppm in a bridging manner allows achievement of the nearly eclipsed configuration. In contrast, dppe in [Fe₂(μ-S(CH₂)₂NⁱPr(CH₂)₂S)(μ-dppe)(CO)₄]₂, **6**, could twist the Fe(CO)_{3-x}L_x fragment to adopt the least strained structure. In addition, the N⋯C(CO_{ap}) interaction would direct the twist towards a specific direction for the closer contact. In return, the shorter N⋯C(CO_{ap}) distance of 3.721(7) Å and larger Φ angle of 26.5° are obtained in **6**. For comparison, 3.987(7) Å and 3.9° of the corresponding parameters are observed in **7**. Conversion of (μ-dppe)[Fe₂(μ-S(CH₂)₂NⁱPr(CH₂)₂S)(CO)₃]₂, **2**, to complex **1** via an associative mechanism is studied.

Introduction

The research of [Fe₂(SR)₂(CO)₆] and its derivatives has been rejuvenated in recent years mainly due to discovery of the active site of Fe-only hydrogenase that consists of a similar {Fe₂S₂} organometallic unit.¹ Numerous synthetic routes have been developed to better model the [2Fe2S] unit within the H-cluster in order to gain understanding of the electrocatalytic mechanism.² In the known synthetic models,³ the phosphine substitution is widely approached to mimic the CN⁻ ligation on the Fe sites in reference to that phosphines are an appropriate σ-donating group which does not lead to polymerization of the diiron units.⁴ A few examples are reported to consist of different σ- or π-type substituents.⁵ Most of the synthetic complexes, however, fail to replicate a key structural feature of the active site of Fe-only hydrogenase, which is proposed as being essential for its high catalytic turnover frequency. One of the Fe moieties of

the enzymatic active center adapts an unusual inverted square pyramid structure.^{6,7} It creates an accessible site for proton reduction/hydrogen oxidation as well as a possible electron-transfer route through a semi-bridging carbonyl group that could mediate electron flux between the Fe^d site and the protein via the cysteinyl bridged [4Fe4S] ferredoxin cluster.⁸

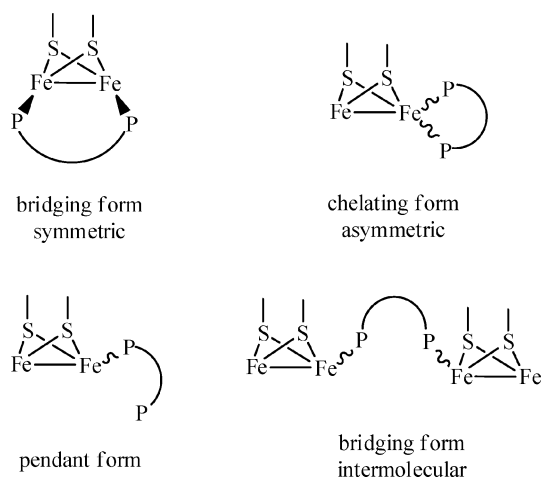
From their theoretical analysis, Hall and Darensbourg recently have suggested the presence of a sterically demanding S–S linker and an asymmetric electronic structure of the Fe sites are effective synthetic targets to achieve the expected inverted geometry of the Fe site.⁹ In the examples of diiron(i) complexes, they have successfully shown the torsion angle (Φ , *vide infra*) between the Fe^I(CO)₃ and Fe^I(CO)₂L units increases from 0.0° of (μ-pdt)[Fe(CO)₃]₂ (pdt = 1,3-propanedithiolate) with the smallest steric bulk to 15.8° of the bulky dithiolate species, (μ-depdt)[Fe(CO)₃]₂ (depdt = 2,2-diethyl-1,3-propanedithiolate). In the presence of larger steric ligands, the torsion angle of 4.26° in (μ-pdt)[Fe(CO)₃][Fe(CO)₂IMes] (IMes = 1,3-bis(2,4,6-trimethylphenyl)imidazol-2-ylidene) is dramatically increased to 40.7° in (μ-dmpdt)[Fe(CO)₃][Fe(CO)₂IMes] (dmpdt = 2,2-dimethyl-1,3-propanedithiolate).¹⁰

Asymmetry of the electronic structure about the Fe^IFe^I centers can be achieved by inequivalent coordination of ligands. In De Gioia's theoretical investigation, the transition state to form the terminal hydride in (μ-edt)[Fe(PH₃)₃][Fe(PH₃)(CO)₂] (edt = 1,2-ethanedithiolate) has a lower energy by 11 kcal mol⁻¹ than

^aInstitute of Chemistry, Academia Sinica, Nankang, Taipei 115, Taiwan^bInstrumentation Center, National Taiwan University, Taipei 106, Taiwan. E-mail: mhchiang@chem.sinica.edu.tw† Electronic supplementary information (ESI) available: A summary of the crystallographic data for complexes **4** and **5** after the SQUEEZE refinement (Table S1). CCDC 793181 (**1**), 793182 (**2**), 793183 (**3**), 793184 (**4**), 793185 (**5**), 793186 (**6**) and 793187 (**7**). For ESI and crystallographic data in CIF or other electronic format see DOI: 10.1039/c0dt01332c

that in $(\mu\text{-edt})[\text{Fe}(\text{PH}_3)_2(\text{CO})_2]$.¹¹ The resultant *t*-hydride species for the former is stabilized by 5 kcal mol⁻¹. Several complexes with unequal arrangement of the ligands have been reported.¹² Most of them are prepared by use of phosphine chelates.¹³ Few have the torsion angle near 30°. Two $\text{Fe}(\text{CO})_{3-x}\text{L}_x$ moieties are twisted by 27.7° in $[\text{Fe}_2(\mu\text{-pdt})(\text{CO})_4(\kappa^2\text{-dppm})]$ (dppm = bis(diphenylphosphino)methane) where both phosphorus atoms are situated at the basal position.¹⁴ In $[\text{Fe}_2(\mu\text{-edt})(\text{CO})_4(\kappa^2\text{-dppv})]$ (dppv = *cis*-1,2-bis(diphenylphosphino)ethylene), the torsion angle is 30.2° and the diphosphine unit is arranged at the apical/basal configuration.¹⁵ If NO^+ is introduced to the same Fe moiety at which the phosphine is located, the twist becomes more significant, reaching 36.1°.¹⁶ The second approach involves a mixed-valent $\text{Fe}^{\text{II}}\text{Fe}^{\text{I}}$ system. Since it is assumed as the H_{ox} state of the active site of Fe-only hydrogenase,¹⁷ many efforts have been paid to explore this type of chemistry. Ligands with better donating ability are used to stabilize the Fe^{II} center. Besides, bulkier substituents are employed to possibly preserve the open site. Pickett,¹⁸ Darenbourg¹⁹ and Rauchfuss²⁰ have reported the formation of thermal sensitive $\text{Fe}^{\text{II}}\text{Fe}^{\text{I}}$ species containing a bridging CO group, which have been characterized by crystallography and spectroscopy.

Substitution reactions of $[\text{Fe}_2(\text{SS})(\text{CO})_6]$ (SS = dithiolate bridges) in the presence of diphosphine ligands have been studied since the 1970s²¹ and recently they received high attention. Coordination configuration of the diphosphines within the Fe_2S_2 moiety depends on various factors: substituent sterics and rigidity of the ligand, and reaction conditions.²² In general, four kinds of species are generated, which are depicted in Scheme 1.



Scheme 1 The coordination mode of a diphosphine ligand.

For example, Rauchfuss *et al.* reported the reaction of $[\text{Fe}_2(\mu\text{-pdt})(\text{CO})_6]$ in the presence of dppv at ambient temperature afforded $[\text{Fe}_2(\mu\text{-pdt})(\text{CO})_4(\kappa^2\text{-dppv})]$.¹⁵ The driving force for formation of the product in the κ^2 -manner is mainly attributed to the rigid *cis*-mode of dppv and thermodynamically-preferred configuration of the five-membered ring. When $[\text{Fe}_2(\mu\text{-odt})(\text{CO})_6]$ (odt = oxadithiolate) reacts with $(\text{Ph}_2\text{PCH}_2\text{CH}_2\text{OCH}_2)_2$ in a ratio of 2 : 1, Song *et al.* isolated $(\text{Ph}_2\text{PCH}_2\text{CH}_2\text{OCH}_2)_2[\text{Fe}_2(\mu\text{-odt})(\text{CO})_5]_2$ as a sole product where the two ends of the phosphine coordinate to two $\{\text{Fe}_2\text{S}_2\}$ units.²³ The length of the ligand backbone also determines the fate: symmetric μ -form *vs.* asymmetric κ^2 -form. For smaller backbones, the acute bite angles would prefer the former

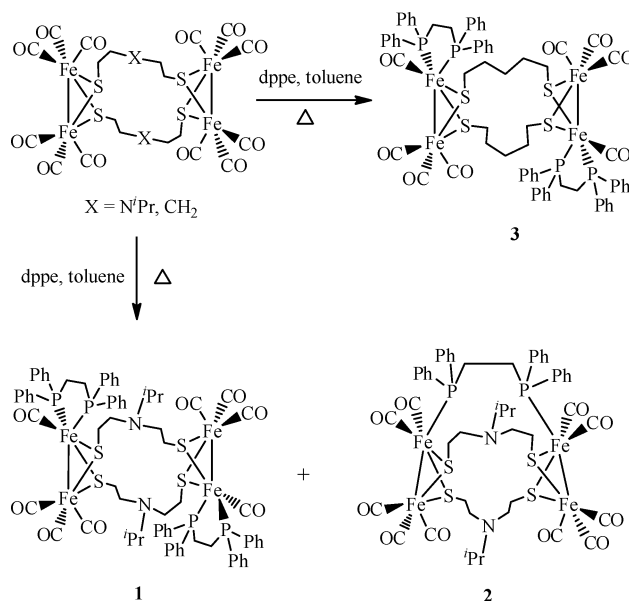
to release the ring strain. On the other hand, too long backbones would inhibit formation of the chelated species due to the high flexibility of the ligand. For dppe (dppe = $\text{Ph}_2\text{P}(\text{CH}_2)_2\text{PPh}_2$), three out of four kinds of species have been observed. In contrast to formation of $(\mu\text{-dppe})[\text{Fe}_2(\text{SS})(\text{CO})_5]_2$ in the presence of limited amount of dppe, $[\text{Fe}_2(\text{SS})(\text{CO})_4(\mu\text{-dppe})]$ is generally afforded in the presence of an excess amount of dppe and under reflux conditions.²⁴⁻²⁶ The κ^2 -dppe substituted species was obtained in the presence of Me_3NO at 70 °C.²⁷

Previously, we have shown that the distance between the aza nitrogen and the apical carbonyl carbon can be treated as a dynamic measure of electron density about the Fe centers.²⁸ Herein, we would like to explore the influence of the aza nitrogen site on the electronic structure of the Fe_2 subunits. Two diphosphine-substituted $\text{Fe}^{\text{I}}\text{Fe}^{\text{I}}$ species in which two Fe moieties are greatly distorted (torsion angle >30°) are reported while lone pairs are not available. Factors such as asymmetric substitution, the presence of the aza nitrogen lone pair and backbones of the bridging phosphines in controlling the deviation from the ideal eclipse configuration are discussed.

Results and discussion

Synthesis and characterization of 1–3

When a toluene solution of $[\text{Fe}_2(\mu\text{-S}(\text{CH}_2)_2\text{N}^i\text{Pr}(\text{CH}_2)_2\text{S})(\text{CO})_6]_2$ was treated with dppe at elevated temperature, two products were isolated (Scheme 2). $[\text{Fe}_2(\mu\text{-S}(\text{CH}_2)_2\text{N}^i\text{Pr}(\text{CH}_2)_2\text{S})(\text{CO})_4(\kappa^2\text{-dppe})]_2$, **1**, as an olive green solid in toluene was separated from the solution. $(\mu\text{-dppe})[\text{Fe}_2(\mu\text{-S}(\text{CH}_2)_2\text{N}^i\text{Pr}(\text{CH}_2)_2\text{S})(\text{CO})_5]_2$, **2**, with higher solubility was purified *via* column chromatography. It is reported that the refluxed reactions of the pdt and adt analogues in the presence of dppe gave $[\text{Fe}_2(\mu\text{-xdt})(\text{CO})_4(\mu\text{-dppe})]$.^{24,25} In contrast, the identifiable product for $[\text{Fe}_2(\mu\text{-S}(\text{CH}_2)_2\text{N}^i\text{Pr}(\text{CH}_2)_2\text{S})(\text{CO})_6]_2$ in the similar condition is complex **1**. It is tentatively suggested that its poor solubility inhibits rearrangement of the κ^2 species to the μ -isomer in the



Scheme 2

Table 1 A list of ν_{CO} bands of complexes **1–8** and selected related diphosphine complexes in CH_2Cl_2

Complex	$\nu_{\text{CO}}/\text{cm}^{-1}$	$\Delta\nu_{\text{CO}}^a/\text{cm}^{-1}$
$[\text{Fe}_2(\mu\text{-S}(\text{CH}_2)_2\text{N}^i\text{Pr}(\text{CH}_2)_2\text{S})(\text{CO})_4(\kappa^2\text{-dppe})]_2$, 1	2016, 1944, 1895	121
$(\mu\text{-dppe})[\text{Fe}_2(\mu\text{-S}(\text{CH}_2)_2\text{N}^i\text{Pr}(\text{CH}_2)_2\text{S})(\text{CO})_5]_2$, 2	2041, 1985, 1971, 1960, 1929	112
$[\text{Fe}_2(\mu\text{-S}(\text{CH}_2)_2\text{S})(\text{CO})_4(\kappa^2\text{-dppe})]_2$, 3	2017, 1943, 1894	123
$[\text{Fe}_2(\mu\text{-S}(\text{CH}_2)_2\text{N}^i\text{Pr}(\text{H})(\text{CH}_2)_2\text{S})(\text{CO})_4(\kappa^2\text{-dppe})]_2^{2+}$, 4	2024, 1958, 1945, 1904	120
$[\text{Fe}_2(\mu\text{-S}(\text{CH}_2)_2\text{N}^i\text{Pr}(\text{Me})(\text{CH}_2)_2\text{S})(\text{CO})_4(\kappa^2\text{-dppe})]_2^{2+}$, 5	2026, 1961, 1940, 1907	119
$[\text{Fe}_2(\mu\text{-S}(\text{CH}_2)_2\text{N}^i\text{Pr}(\text{CH}_2)_2\text{S})(\mu\text{-dppe})(\text{CO})_4]_2$, 6	1982, 1954, 1914, 1891	91
$[\text{Fe}_2(\mu\text{-S}(\text{CH}_2)_2\text{N}^i\text{Pr}(\text{CH}_2)_2\text{S})(\mu\text{-dppm})(\text{CO})_4]_2$, 7	1982, 1958, 1916, 1899	83
$[\text{Fe}_2(\mu\text{-S}(\text{CH}_2)_2\text{S})(\mu\text{-dppe})(\text{CO})_4]_2$, 8	1983, 1955, 1917, 1898	85
$[\text{Fe}_2(\mu\text{-edt})(\text{CO})_4(\kappa^2\text{-dppv})]^{15}$	2023, 1953, 1915	108
$[\text{Fe}_2(\mu\text{-pdt})(\text{CO})_4(\kappa^2\text{-PNP})]^{22}$	2019, 1939, 1908 ^b	111
$[\text{Fe}_2(\mu\text{-pdt})(\text{CO})_4(\kappa^2\text{-dppm})]^{14}$	2023, 1952, 1917 ^c	106
$[\text{Fe}_2(\mu\text{-pdt})(\text{CO})_4(\mu\text{-dppe})]^{24}$	1990, 1953, 1920, 1902	88
$[\text{Fe}_2(\mu\text{-pdt})(\text{CO})_4(\mu\text{-dcpm})]^{14}$	1975, 1942, 1906, 1889 ^d	86

^a The energy difference between the highest energy and the lowest energy ν_{CO} bands. ^b In CH_3CN solution. PNP = $(\text{EtO})_2\text{PN}(\text{Me})\text{P}(\text{OEt})_2$. ^c In hexane solution. ^d dcpm = $(\text{C}_6\text{H}_{11})_2\text{PCH}_2\text{P}(\text{C}_6\text{H}_{11})_2$.

solution. $[\text{Fe}_2(\mu\text{-S}(\text{CH}_2)_2\text{S})(\text{CO})_4(\kappa^2\text{-dppe})]_2$, **3**, was isolated from the similar reaction with $[\text{Fe}_2(\mu\text{-S}(\text{CH}_2)_2\text{S})(\text{CO})_6]_2$. No evidence of $(\mu\text{-dppe})[\text{Fe}_2(\mu\text{-S}(\text{CH}_2)_2\text{S})(\text{CO})_5]_2$ and $[\text{Fe}_2(\mu\text{-S}(\text{CH}_2)_2\text{S})(\text{CO})_4(\mu\text{-dppe})]_2$ was observed. Different reactivity towards dppm has been reported for the pdt and adt analogues.²⁹ Combined with the current results, this may suggest the bridgehead of the dithiolate linkers being a non-innocent role in the substitution reactions.

The IR spectra of complexes **1** and **3** feature three ν_{CO} bands each, consistent with the $\{\text{Fe}_2\text{S}_2\}$ core wherein dppe is chelated to one Fe center. Energies of the ν_{CO} bands for both complexes are lower than their pdt analogues. The IR results are tabulated in Table 1 together with those of the related diphosphine chelated complexes for comparison. DFT calculations have suggested that energies of the highest and lowest ν_{CO} bands are an approximate gauge of electron richness about the $\text{Fe}(\text{CO})_3$ and $\text{Fe}(\text{CO})\text{P}_2$ moieties.¹⁵ The difference of these two bands could be a measure of electron asymmetry between the P-substituted and unsubstituted fragments. The values of $\Delta\nu_{\text{CO}}$ for **1** and **3** are greater than 120 cm^{-1} , which is larger than the values of the xdt analogues, 110 cm^{-1} .^{14,24,27,30} Interestingly, such large difference is usually observed in the mono-substituted derivatives.³¹ For the sake of comparison, $\Delta\nu_{\text{CO}}$ is $70\text{--}90\text{ cm}^{-1}$ for the symmetrically diphosphine species.³²

X-Ray crystallographic analyses of **1–3** were carried out at 150 K. Their molecular structures are displayed in Fig. 1–3 and selected metric parameters are included in the figure captions. All three complexes have a dimer-of-dimer structure, wherein each dimer composes of a $\{\text{Fe}_2\text{S}_2\}$ unit that resembles the active site of Fe-only hydrogenase. Each Fe center within the $\{\text{Fe}_2\text{S}_2\}$ moiety is coordinated by five ligands and the metal–metal bond completes the distorted octahedral coordination geometry. For complexes **1** and **3**, the dppe ligand is coordinated to one of the Fe sites *via* the chelated mode, leaving the other $\{\text{Fe}(\text{CO})_3\}$ fragment intact. Two P atoms arrange at the apical/basal configuration, which has been confirmed by ³¹P NMR spectroscopy (83.2 and 85.5, and 84.4 and 85.3 ppm for **1** and **3**, respectively). For complex **2**, the dppe ligand bridges two dimeric units within the molecule. Two ends of the diphosphine coordinate to the apical sites, which pulls two P substituted sides close to each other. Only one ³¹P signal at 54.1 ppm was recorded at the NMR spectrum of 243 K. When it was increased to ambient temperature, an

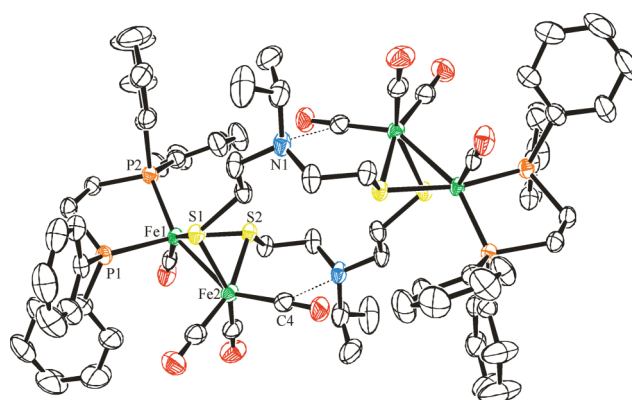


Fig. 1 Molecular structure of $[\text{Fe}_2(\mu\text{-S}(\text{CH}_2)_2\text{N}^i\text{Pr}(\text{CH}_2)_2\text{S})(\text{CO})_4(\kappa^2\text{-dppe})]_2$, **1**, thermal ellipsoids drawn at 30% probability level. All hydrogen atoms are omitted for clarity. Selected bond lengths (Å) and angles ($^\circ$): Fe–Fe, 2.5406(5); Fe–S, 2.2736(8); Fe–P, 2.2024(8); Fe–C_{CO,ap}, 1.805(3); Fe–C_{CO,ba}, 1.758(3); S–Fe–S, 79.64(3); S–Fe–Fe, 56.04(2); Fe–S–Fe, 67.93(2).

additional resonance from its isomer at 58.4 ppm appeared in a quantitative intensity. Distances of the metal–metal bond for complexes **1** and **3** are similar (2.54 vs. 2.55 Å). For **2**, the distance is shorter by about 0.03 Å. Sums of the angles about the aza nitrogen site are 339.7 and 341.9 on average for **1** and **2**, respectively. These indicate the presence of sp^3 N site and in turn availability of its lone pair. The distance between the aza nitrogen and the closest apical carbonyl carbon is 3.796(4) Å in **1**, which is shorter than the averaged value of 4.011(3) Å in its parent molecule, $[\text{Fe}_2(\mu\text{-S}(\text{CH}_2)_2\text{N}^i\text{Pr}(\text{CH}_2)_2\text{S})(\text{CO})_6]_2$.²⁸ In **2**, the dppe bridge between two separated $\{\text{Fe}_2\text{S}_2\}$ units constructs a basket-like structure. No similar $\text{N}\cdots\text{C}(\text{CO}_{\text{ap}})$ distance less than 4 Å is observed.

Conversion of **2** to **1**

When complex **2** was reacted with dppe, **1** was generated. The reaction occurs at room temperature at a slow rate. Prolonged reaction time causes decomposition of the complexes. Fig. 4 displays the IR spectra recorded for the reaction of **2** in the presence of 1 equiv. of dppe at 55 °C in a THF solution. Intensities of the IR signatures of **2** at 2042, 1986, 1977, 1962,

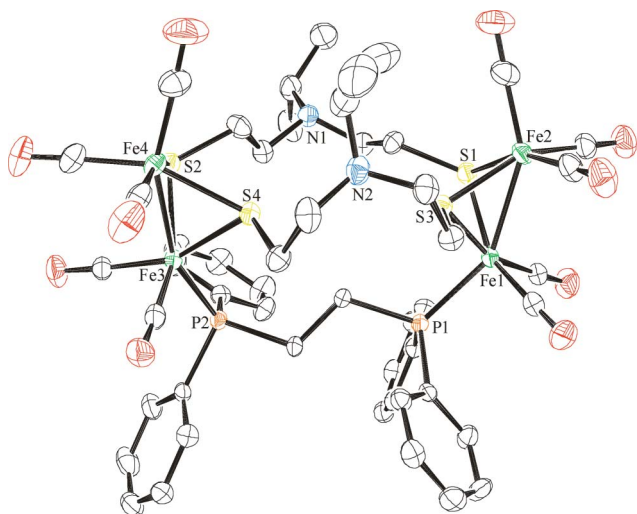


Fig. 2 Molecular structure of $(\mu\text{-dppe})[\text{Fe}_2(\mu\text{-S}(\text{CH}_2)_2\text{N}^i\text{Pr}(\text{CH}_2)_2\text{S})(\text{CO})_5]_2$, **2**, thermal ellipsoids drawn at 50% probability level. All hydrogen atoms are omitted for clarity. Selected bond lengths (\AA) and angles ($^\circ$): Fe–Fe, 2.5076(7); Fe–S, 2.2722(10); Fe–P, 2.2252(10); Fe–C_{CO,ap}, 1.810(5); Fe–C_{CO,ba}, 1.777(4); S–Fe–S, 79.67(3); S–Fe–Fe, 56.51(3); Fe–S–Fe, 67.98(3).

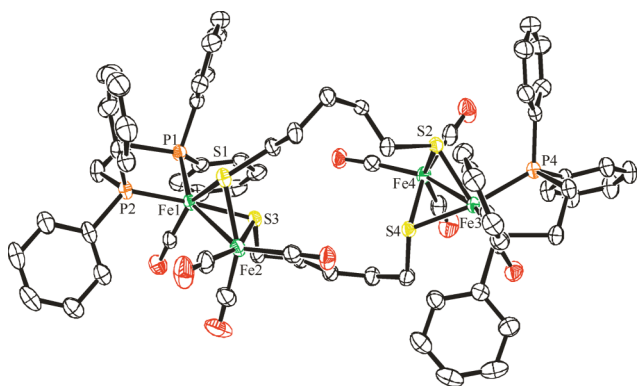


Fig. 3 Molecular structure of $[\text{Fe}_2(\mu\text{-S}(\text{CH}_2)_2\text{S})(\text{CO})_4(\kappa^2\text{-dppe})]_2$, **3**, thermal ellipsoids drawn at 50% probability level. All hydrogen atoms are omitted for clarity. Selected bond lengths (\AA) and angles ($^\circ$): Fe–Fe, 2.5488(4); Fe–S, 2.2648(6); Fe–P, 2.1991(6); Fe–C_{CO,ap}, 1.810(2); Fe–C_{CO,ba}, 1.763(3); S–Fe–S, 80.21(2); S–Fe–Fe, 55.759(16); Fe–S–Fe, 68.483(18).

1936, 1928 cm^{-1} decrease while the IR bands of **1** (1917, 1947, 1897 cm^{-1}) increase with time. Their intensities only reach a maximum and then the product is precipitated due to limited solubility of complex **1**. Decomposition occurred without formation of complex **1** while the ligand was absent. This suggests complex **2** is one of the intermediates in the reaction of $[\text{Fe}_2(\mu\text{-S}(\text{CH}_2)_2\text{N}^i\text{Pr}(\text{CH}_2)_2\text{S})(\text{CO})_6]_2$ and dppe to the formation of **1**. On the basis of the larger Φ angle (*vide infra*), it is tentatively assumed that energy barrier to the rotation of the $\text{Fe}(\text{CO})_3$ moiety is lowered in **2**. The phosphine coordination and the turnstile rotation of the $\text{Fe}(\text{CO})_3$ moiety occur in a concerted manner, concomitant with formation of a bridging or semi-bridging CO group. The subsequent CO migration results in formation of the pendant species, $[\text{Fe}_2(\mu\text{-S}(\text{CH}_2)_2\text{N}^i\text{Pr}(\text{CH}_2)_2\text{S})(\text{CO})_5(\kappa^1\text{-dppe})]_2$. Decarbonylation and chelation of the dppe ligand lead to complex **1**. It is assumed either this pendant complex **A** is a short-

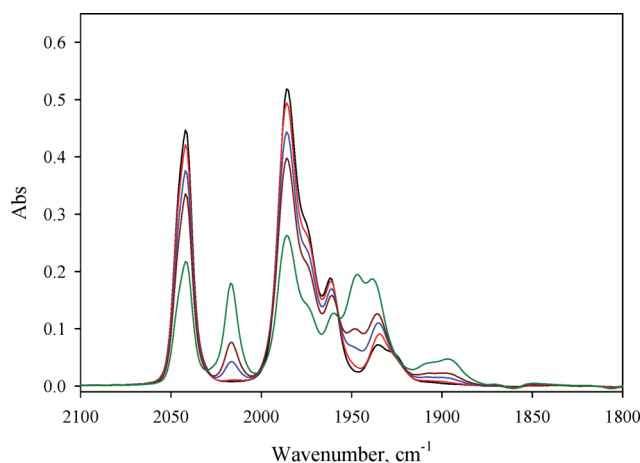
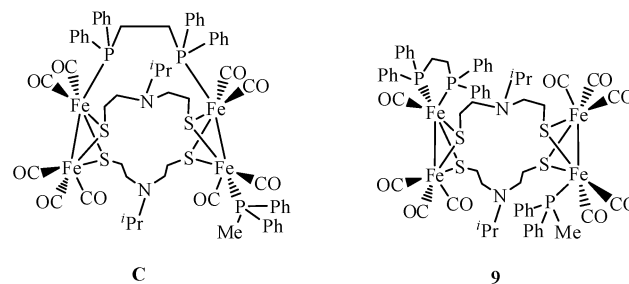


Fig. 4 IR spectra for the reaction of $(\mu\text{-dppe})[\text{Fe}_2(\mu\text{-S}(\text{CH}_2)_2\text{N}^i\text{Pr}(\text{CH}_2)_2\text{S})(\text{CO})_5]_2$ with 1 equiv. of dppe in a THF solution at 55 $^\circ\text{C}$. The IR spectra recorded at 0, 1, 3, 5 and 22 h are shown.

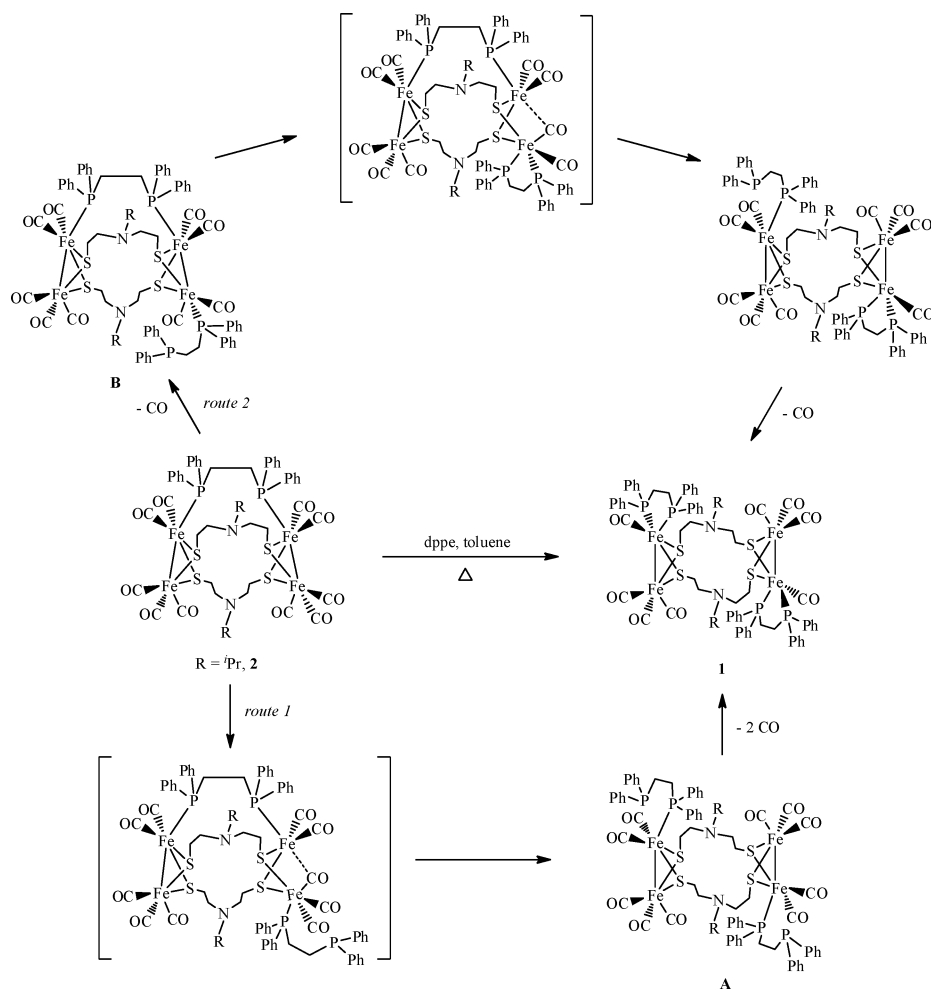
lived species since no apparent evidence is observed for its presence in the IR and ^{31}P NMR spectra or the following steps: Fe–P bond breaking, CO migration and P-chelation occur simultaneously. The proposed conversion mechanism is displayed as route 1 in Scheme 3.

A different reaction route can be proposed if **2** is treated as a complex of two $\{\text{Fe}(\text{CO})_5\text{P}\}$ subunits. It is well known that reactions of $[\text{Fe}_2(\mu\text{-SS})(\text{CO})_5\text{P}_1]$ and P_2 (P_1 , P_2 = monodentate phosphines) lead to formation of disubstituted products, $(\mu\text{-SS})[\text{Fe}(\text{CO})_2\text{P}_1][\text{Fe}(\text{CO})_2\text{P}_2]$.³³ In the conversion of **2** to **1**, the exogenous dppe ligand could substitute one of the CO groups *via* monodentate coordination to the Fe center, which is followed by coordination of the second P end and CO migration (route 2 in Scheme 3). Since identification of the pendant species, complex **B**, is not feasible, dppe is replaced by PPh_2Me to confirm whether formation of the similar species of **B**, complex **C** occurs. Instead, complex **9** is generated, shown in Fig. 5. The results suggest that the CO-bridge mechanism of route 1 which opens up a site for the P coordination is favored over the CO-substitution mechanism (route 2) in the initial step.



Distortion of the ideal eclipse configuration

Electronic asymmetry vs. the aza nitrogen bridgehead. The idealized structure in $[\text{Fe}_2(\text{SR})_2(\text{CO})_6]$ possesses a C_{2v} symmetry. Theoretical calculations show that two Fe centers have equal Mulliken charges. If one of the $\text{Fe}(\text{CO})_3$ moieties is rotated by 60° , subsequent breaking of the metal–metal bonding and asymmetric distribution of Mulliken charges occur.³⁴ It would be interesting to examine our complexes by the Ψ angle, which is the angle between



Scheme 3

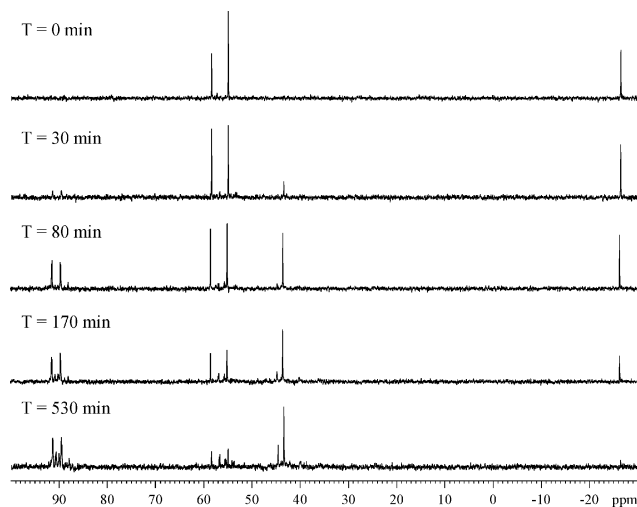
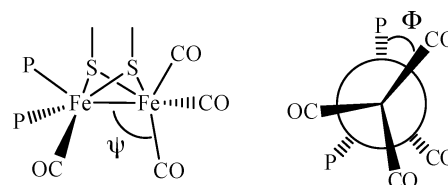


Fig. 5 ^{31}P NMR spectra recorded over the course of 10 h for the reaction of **2** and PPh_2Me in toluene at 45°C . The signal at -26.47 ppm is from PPh_2Me .

the Fe–Fe vector and the CO group underneath it defined by Crabtree,³⁵ displayed in Scheme 4. A typical value around 100° is observed for the terminal carbonyl, whereas the Ψ angle decreases



Scheme 4

as the carbonyl spins about the Fe–Fe axis to form a bent CO bridge. From the $\Delta\nu_{\text{CO}}$ value, it is expected dissimilarity of electron density between the $\text{Fe}(\text{CO})_3$ and $\text{Fe}(\text{CO})\text{P}_2$ moieties in complex **1** is significant but a Ψ value of 97.9° is observed (Table 2). The main reason for this result could be attributed to the aza nitrogen factor. Since the IR spectra were recorded at ambient temperature, the thermal energy has overcome the weak $\text{N}\cdots\text{C}(\text{CO}_{\text{ap}})$ interaction and the ν_{CO} bands are the averaged result of fluxional behavior of the CO groups, which directly reflects dissimilarity of electron density. On the other hand, the crystallographic data was collected at 150 K. The fluxional mechanism of the CO groups has been shut down at this temperature. In view of its pointing towards the apical carbonyl and the shorter $\text{N}\cdots\text{C}(\text{CO}_{\text{ap}})$ distance, the presence of the N lone pair is possibly in control of rotation of the $\text{Fe}(\text{CO})_3$ subunit.

Table 2 A list of complexes 1–7 and the related diphosphine complexes with $\Phi > 25^\circ$ or $\Psi < 95^\circ$

Complex	$\Phi^a / ^\circ$	$\Psi^b / ^\circ$
$[\text{Fe}_2(\mu\text{-S}(\text{CH}_2)_2\text{N}^i\text{Pr}(\text{CH}_2)_2\text{S})(\text{CO})_4(\kappa^2\text{-dppe})]_2$, 1	10.8	97.9
$(\mu\text{-dppe})[\text{Fe}_2(\mu\text{-S}(\text{CH}_2)_2\text{N}^i\text{Pr}(\text{CH}_2)_2\text{S})(\text{CO})_5]_2$, 2	20.7	98.5
	13.2 ^c	96.8
$[\text{Fe}_2(\mu\text{-S}(\text{CH}_2)_2\text{S})(\text{CO})_4(\kappa^2\text{-dppe})]_2$, 3	6.8	98.9
	0.8 ^c	96.6
$[\text{Fe}_2(\mu\text{-S}(\text{CH}_2)_2\text{N}^i\text{Pr}(\text{H})(\text{CH}_2)_2\text{S})(\text{CO})_4(\kappa^2\text{-dppe})]_2^{2+}$, 4	34.1 (33.7) ^c	91.4 (91.4) ^c
$[\text{Fe}_2(\mu\text{-S}(\text{CH}_2)_2\text{N}^i\text{Pr}(\text{Me})(\text{CH}_2)_2\text{S})(\text{CO})_4(\kappa^2\text{-dppe})]_2^{2+}$, 5	36.3 (36.0) ^c	85.9 (85.9) ^c
	34.5 ^c (35.8) ^c	99.6 (99.3) ^c
$[\text{Fe}_2(\mu\text{-S}(\text{CH}_2)_2\text{N}^i\text{Pr}(\text{CH}_2)_2\text{S})(\mu\text{-dppe})(\text{CO})_4]_2$, 6	26.5	94.4
$[\text{Fe}_2(\mu\text{-S}(\text{CH}_2)_2\text{N}^i\text{Pr}(\text{CH}_2)_2\text{S})(\mu\text{-dppm})(\text{CO})_4]_2$, 7	4.1	99.0
	3.6 ^c	99.8
$[\text{Fe}_2(\mu\text{-edt})(\text{CO})_4(\kappa^2\text{-dppv})]_2^{15}$	30.2	105.1
	12.3 ^d	99.7
$[\text{Fe}_2(\mu\text{-pdt})(\text{CO})_4(\kappa^2\text{-dppm})]_2^{14}$	27.7	99.4
$[\text{Fe}_2(\mu\text{-S}(\text{CH}_2)_2\text{N}^i\text{Pr})(\text{CO})_4(\mu\text{-dppm})]_2^{19}$	31	94.9

^a The angle, $\angle L_{\text{ap}}\text{-Fe-Fe-}L_{\text{ap}}$, is defined by Darensbourg to measure the distortion between two apical ligands. ^b The angle, $\angle \text{Fe-Fe-C}(\text{CO})$, is defined by Crabtree as an indicator for the bent semi-bridging, bridging and terminal carbonyls. ^c Values are taken from two asymmetric Fe_2 units within one molecule. ^d This complex crystallizes with two asymmetric molecules in its unit cell. ^e The values in parentheses are obtained with the SQUEEZE treatment.

$[\text{Fe}_2(\mu\text{-S}(\text{CH}_2)_2\text{N}^i\text{Pr}(\text{H})(\text{CH}_2)_2\text{S})(\text{CO})_4(\kappa^2\text{-dppe})]_2(\text{CF}_3\text{COO})_2$, **[4]** $(\text{CF}_3\text{COO})_2$, and $[\text{Fe}_2(\mu\text{-S}(\text{CH}_2)_2\text{N}^i\text{Pr}(\text{Me})(\text{CH}_2)_2\text{S})(\text{CO})_4(\kappa^2\text{-dppe})]_2(\text{OTf})_2$, **[5]** $(\text{OTf})_2$, respectively were afforded when complex **1** was reacted with TFA (trifluoroacetic acid) and MeOTf (methyl trifluoromethanesulfonate). The molecular structures of both complexes are displayed in Fig. 6 and 7. Their selected metric

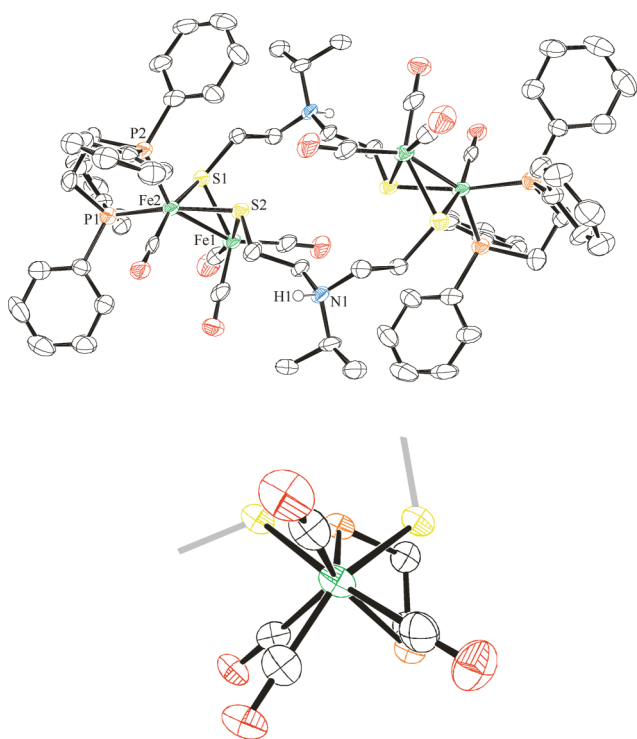


Fig. 6 Molecular structures of $[\text{Fe}_2(\mu\text{-S}(\text{CH}_2)_2\text{N}^i\text{Pr}(\text{H})(\text{CH}_2)_2\text{S})(\text{CO})_4(\kappa^2\text{-dppe})]_2^{2+}$, **4**, thermal ellipsoids drawn at 30% probability level. All hydrogen atoms are omitted for clarity. The side view of partial molecular structure is shown to highlight the distortion. Selected bond lengths (Å) and angles ($^\circ$): Fe–Fe, 2.5946(17); Fe–S, 2.273(3); Fe–P, 2.215(3); Fe–C_{CO,ap}, 1.811(10); Fe–C_{CO,ba}, 1.764(10); S–Fe–S, 81.45(9); S–Fe–Fe, 55.19(7); Fe–S–Fe, 69.62(8).

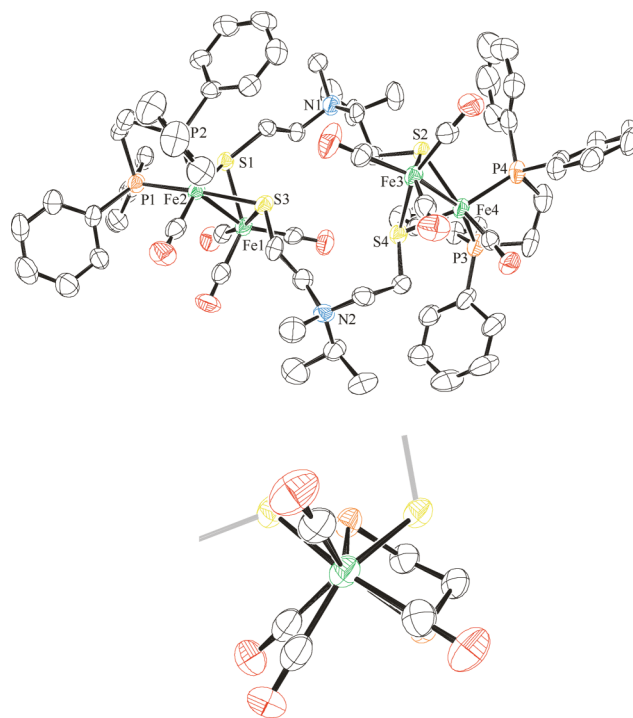


Fig. 7 Molecular structures of $[\text{Fe}_2(\mu\text{-S}(\text{CH}_2)_2\text{N}^i\text{Pr}(\text{Me})(\text{CH}_2)_2\text{S})(\text{CO})_4(\kappa^2\text{-dppe})]_2^{2+}$, **5**, thermal ellipsoids drawn at 30% probability level. All hydrogen atoms are omitted for clarity. The side view of partial molecular structure is shown to highlight the distortion. Selected bond lengths (Å) and angles ($^\circ$): Fe–Fe, 2.5444(19); Fe–S, 2.272(3); Fe–P, 2.215(3); Fe–C_{CO,ap}, 1.795(12); Fe–C_{CO,ba}, 1.773(13); S–Fe–S, 80.26(10); S–Fe–Fe, 55.95(8); Fe–S–Fe, 68.11(9).

parameters are listed in the corresponding figure captions. The presence of the protonated and methylated aza N sites provides an opportunity to examine the possible involvement of the N lone pair on the Ψ angle. In complex **4**, it decreases to 91.4° and a smaller Ψ value, 85.9° , is obtained for complex **5**.

The second parameter can be used to evaluate the extent of electron asymmetry. The Φ angle is defined as the torsion angle

of $L_{ap}\text{-Fe-Fe-L}_{ap}$, introduced by Darensbourg, Scheme 4.¹⁰ This value is practically zero in $[\text{Fe}_2(\mu\text{-pdt})(\text{CO})_6]$ and increases to 15.8° for the bulky bridgehead derivative, $(\mu\text{-depdt})[\text{Fe}(\text{CO})_3]_2$. In combination of inequivalent substitution, the Φ angle reaches 40.7° in $(\mu\text{-dmpdt})[\text{Fe}(\text{CO})_3][\text{Fe}(\text{CO})_2\text{IMes}]$. For the current work if the steric influence is diminished to the minimum such as in the protonated and methylated species the N sites are swung away from the $\text{Fe}(\text{CO})_3$ subunits, the Φ angle would practically reflect the electronic dissimilarity in complexes **4** and **5**. Up to date, including complexes **4** and **5**, only four κ^2 -diphosphine Fe^IFe^I carbonyl dithiolate complexes that possess the Φ angle close to or larger than 30° are characterized (Table 2). Compared with $[\text{Fe}_2(\mu\text{-edt})(\text{CO})_4(\kappa^2\text{-dppv})]$ ($\Phi = 30.2^\circ$)¹⁵ and $[\text{Fe}_2(\mu\text{-pdt})(\text{CO})_4(\kappa^2\text{-dppm})]$ ($\Phi = 27.7^\circ$),¹⁴ complexes **4** ($\Phi = 34.1^\circ$) and **5** ($\Phi = 36.3^\circ$) have the most distorted $\text{Fe}(\text{CO})_3$ centers.

The bridging phosphine vs. the aza nitrogen bridgehead. Dppe is a diphosphine ligand that consists of a two-carbon backbone. This gives the ligand a higher degree of freedom to adopt the least strained structure when dppe bridges two Fe centers. For comparison, the distance between two phosphorus atoms within the Fe_2 subunits of $[\text{Fe}_2(\mu\text{-S}(\text{CH}_2)_2\text{N}^i\text{Pr}(\text{CH}_2)_2\text{S})(\mu\text{-dppe})(\text{CO})_4]_2$, **6**, is 3.787 \AA while the distances of the two basal carbonyl carbons and Fe–Fe bond are 3.137 and 2.549 \AA , respectively. A twist away from the eclipsed configuration between two $\text{Fe}(\text{CO})_2\text{P}$ moieties is observed in **6**, as displayed in Fig. 8a. The Φ angle is measured to 26.5° (Scheme 5). The $\text{N} \cdots \text{C}(\text{CO}_{ap})$ interaction could facilitate the rotation as well. Compared with $4.011(3) \text{ \AA}$ of the parent molecule, $[\text{Fe}_2(\mu\text{-S}(\text{CH}_2)_2\text{N}^i\text{Pr}(\text{CH}_2)_2\text{S})(\text{CO})_6]_2$,²⁸ a shorter $\text{N} \cdots \text{C}(\text{CO}_{ap})$ distance of $3.721(7) \text{ \AA}$ is observed. The $\text{N} \cdots \text{C}(\text{CO}_{ap})$ interaction is expected as an additive factor that would conduct the twist towards a specific direction for the closer contact between the apical carbonyl and the aza nitrogen. This phenomenon would tentatively explain the small Φ angles in the other dppe related species: 8 and 6.5° for $[\text{Fe}_2(\mu\text{-SCH}_2\text{N}^i\text{Pr}(\text{CH}_2)_2\text{S})(\mu\text{-dppe})(\text{CO})_4]$ ³⁰ and $[\text{Fe}_2(\mu\text{-pdt})(\mu\text{-dppe})(\text{CO})_4]$,²⁶ respectively. Repulsion due to steric bulk of the ^iPr substituent overcomes stabilization from the anomeric effect.³⁶ This enforces the alkyl group to the equatorial position, leaving the lone pair of the aza nitrogen at the axial position close to the apical carbonyl. The possible $\text{N} \cdots \text{C}(\text{CO}_{ap})$ and $\text{H}(\text{CH}_2) \cdots \text{O}(\text{CO}_{ap})$ interactions could dictate the almost eclipsed configuration within these two species. The “Newman projections” in Scheme 5 provide a clear representation how the $\text{N} \cdots \text{C}(\text{CO}_{ap})$ and $\text{H}(\text{CH}_2) \cdots \text{O}(\text{CO}_{ap})$ interactions could influence stereochemistry of the species.

On the other hand, the $\text{Fe}_2(\text{CO})_4\text{P}_2$ unit with a dppm bridge has the more compact structure: 2.522 and 2.549 \AA for the Fe–Fe bond distances in $[\text{Fe}_2(\mu\text{-S}(\text{CH}_2)_2\text{N}^i\text{Pr}(\text{CH}_2)_2\text{S})(\mu\text{-dppm})(\text{CO})_4]_2$, **7**, (Fig. 8b) and complex **6**, respectively. Dppm is a relatively rigid bridging ligand that allows the eclipsed configuration to be achieved. In other words, the comparable Φ angle and $\text{N} \cdots \text{C}(\text{CO}_{ap})$ distance are expected between the dppm-substituted derivatives and the all-CO molecules: 3.9 (av.) vs. 6.0° and $3.987(7)$ vs. $4.011(3) \text{ \AA}$ for **7** and $[\text{Fe}_2(\mu\text{-S}(\text{CH}_2)_2\text{N}^i\text{Pr}(\text{CH}_2)_2\text{S})(\text{CO})_6]_2$, respectively (Scheme 6). For comparison, the $\text{Fe}(\text{CO})_2\text{P}$ moieties in $[\text{Fe}_2(\mu\text{-pdt})(\mu\text{-dppm})(\text{CO})_4]$ are twisted by 5.2° .²⁹ Interestingly, one exception is found in $[\text{Fe}_2(\mu\text{-SCH}_2\text{N}^i\text{Pr}(\text{CH}_2)_2\text{S})(\mu\text{-dppm})(\text{CO})_4]$ in which the twist angle is as large as 31° .²⁹ In contrast to other adt analogues, the alkyl substituent in this species is located at the

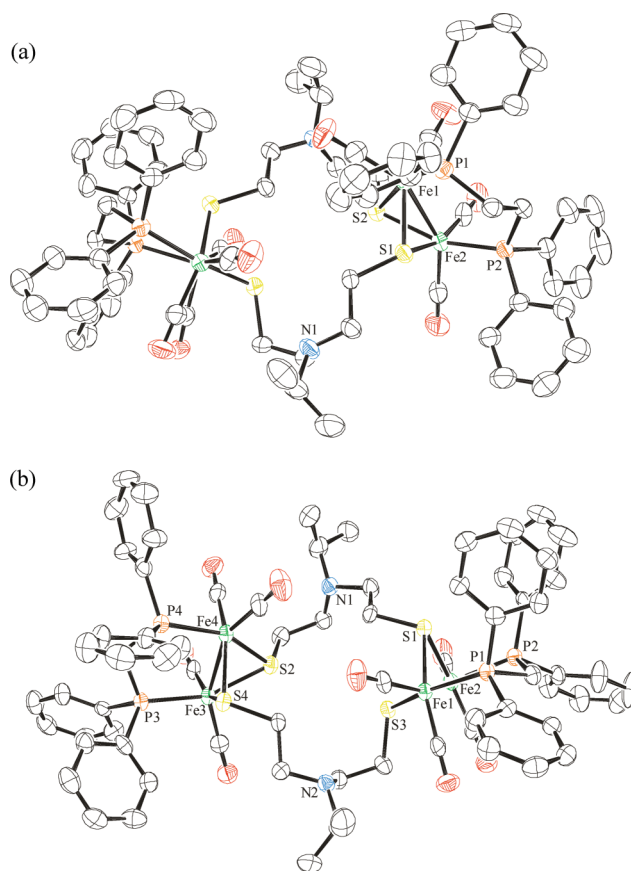
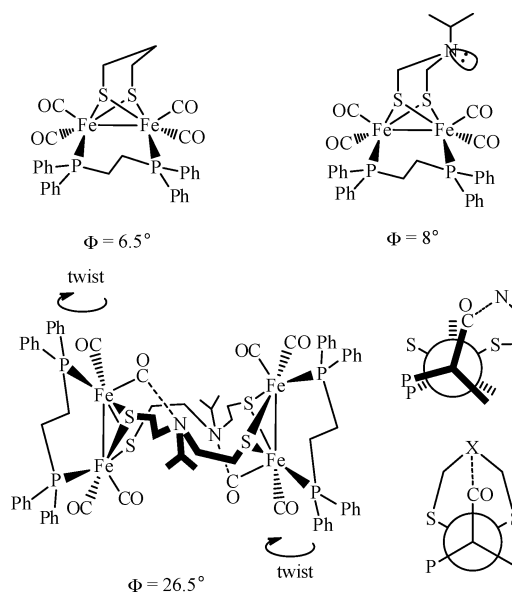


Fig. 8 Molecular structures of $[\text{Fe}_2(\mu\text{-S}(\text{CH}_2)_2\text{N}^i\text{Pr}(\text{CH}_2)_2\text{S})(\text{CO})_4(\mu\text{-L})]_2$ ((a) $L = \text{dppe}$, **6**; (b) $L = \text{dppm}$, **7**), thermal ellipsoids drawn at 30% probability level. All hydrogen atoms are omitted for clarity. Selected bond lengths (\AA) and angles ($^\circ$) for **6**: Fe–Fe, 2.5485(9); Fe–S, 2.2604(12); Fe–P, 2.2111(13); Fe– $\text{C}_{\text{CO}_{ap}}$, 1.785(5); Fe– $\text{C}_{\text{CO}_{ba}}$, 1.761(5); S–Fe–S, 80.52(4); S–Fe–Fe, 55.69(3); Fe–S–Fe, 68.63(4); for **7**: Fe–Fe, 2.5222(10); Fe–S, 2.2622(15); Fe–P, 2.2141(15); Fe– $\text{C}_{\text{CO}_{ap}}$, 1.772(6); Fe– $\text{C}_{\text{CO}_{ba}}$, 1.751(6); S–Fe–S, 80.10(5); S–Fe–Fe, 56.12(4); Fe–S–Fe, 67.77(4).

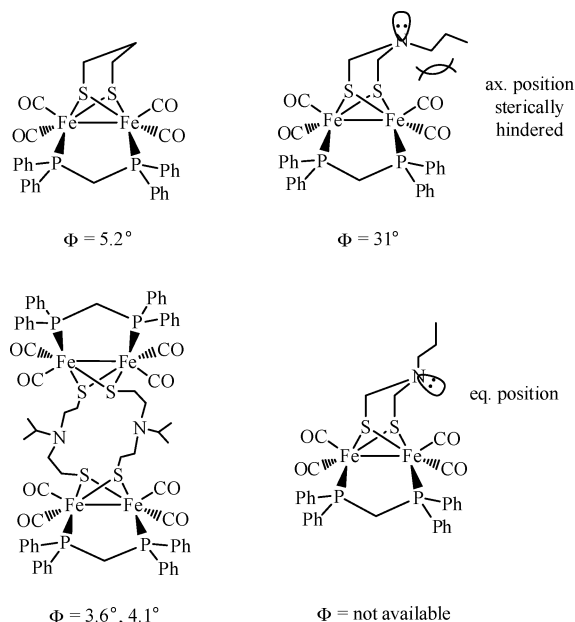


Scheme 5

Table 3 Electrochemical properties of complexes **1–8** (1 mM in THF, 0.1 M $n\text{Bu}_4\text{PF}_6$, $\nu = 100 \text{ mV s}^{-1}$)

Complex	Oxidation potential/V (vs. Fc/Fc^+)	Reduction potential/V (vs. Fc/Fc^+)
$[\text{Fe}_2(\mu\text{-S}(\text{CH}_2)_2\text{N}^i\text{Pr}(\text{CH}_2)_2\text{S})(\text{CO})_4(\kappa^2\text{-dppe})_2]$, 1	0.38, ^a 0.28, ^a -0.08, -0.29	-2.44, -2.64, ^a -2.80 ^b
$(\mu\text{-dppe})[\text{Fe}_2(\mu\text{-S}(\text{CH}_2)_2\text{N}^i\text{Pr}(\text{CH}_2)_2\text{S})(\text{CO})_5]$, 2	0.58, 0.46	-2.15, -2.28, -2.59 ^b
$[\text{Fe}_2(\mu\text{-S}(\text{CH}_2)_2\text{S})(\text{CO})_4(\kappa^2\text{-dppe})_2]$, 3	0.57, ^b 0.35, ^a -0.07, -0.2	-2.36, -2.60, ^a -2.74 ^b
$[\text{Fe}_2(\mu\text{-S}(\text{CH}_2)_2\text{N}^i\text{Pr}(\text{H})(\text{CH}_2)_2\text{S})(\text{CO})_4(\kappa^2\text{-dppe})_2]^{2+}$, 4	0.44, ^a 0.04, ^a -0.04	-2.09, -2.46, ^c -2.61, ^a -2.78 ^b
$[\text{Fe}_2(\mu\text{-S}(\text{CH}_2)_2\text{N}^i\text{Pr}(\text{Me})(\text{CH}_2)_2\text{S})(\text{CO})_4(\kappa^2\text{-dppe})_2]^{2+}$, 5	0.54, ^b 0.19	-1.89, -2.15, -2.40, -2.61, -2.78 ^b
$[\text{Fe}_2(\mu\text{-S}(\text{CH}_2)_2\text{N}^i\text{Pr}(\text{CH}_2)_2\text{S})(\mu\text{-dppe})(\text{CO})_4]$, 6	0.4, 0.29, 0.09	-2.59, -2.73 ^b
$[\text{Fe}_2(\mu\text{-S}(\text{CH}_2)_2\text{N}^i\text{Pr}(\text{CH}_2)_2\text{S})(\mu\text{-dppm})(\text{CO})_4]$, 7	0.42, 0.14	-2.52, -2.65 ^b
$[\text{Fe}_2(\mu\text{-S}(\text{CH}_2)_2\text{S})(\mu\text{-dppe})(\text{CO})_4]$, 8	0.36, 0.15	-2.56, -2.72 ^b

^a Responses from the μ -species. ^b Quasi-reversible, inhibited under CO atmosphere. ^c Responses from the κ^2 -species.

**Scheme 6**

axial position. It exerts a large steric influence that repels the nearby apical carbonyl. A similar observation has been reported in the $[\text{Fe}_2(\mu\text{-SS})(\text{CO})_6]$ series (SS = pdt, depdt).¹⁰ No example with an equatorial alkyl substituent is available for comparison.

Electrochemistry

Cyclic voltammograms of $[\text{Fe}_2(\mu\text{-S}(\text{CH}_2)_2\text{X}(\text{CH}_2)_2\text{S})(\text{CO})_4(\kappa^2\text{-dppe})_2]$ ($\text{X} = \text{N}^i\text{Pr}$, **1**; CH_2 , **3**) at room temperature in the accessible electrochemical window of THF under N_2 exhibit two irreversible reduction processes and one quasi-reversible reduction event at the most negative potential in the absence of any acid (Table 3 and Fig. 9). The first reduction waves recorded at -2.44 and -2.36 V are assigned to the reduction of **1** and **3**, respectively (all potentials in this paper are vs. Fc/Fc^+). Recently, it is reported that electrocatalytic isomerization of the κ^2 -species occurs to form the μ -species.³⁰ On the basis of the electrochemical behavior of complexes **1** and **3**, the same electron transfer-catalyzed (ETC) process is expected. $[\text{Fe}_2(\mu\text{-S}(\text{CH}_2)_2\text{X}(\text{CH}_2)_2\text{S})(\mu\text{-dppe})(\text{CO})_4]$ ($\text{X} = \text{N}^i\text{Pr}$, **6**; CH_2 , **8**) in quantitative yields were obtained from controlled-potential electrolysis of the corresponding κ^2 -species. The molecular structure of complex **6** is shown in Fig. 8a and

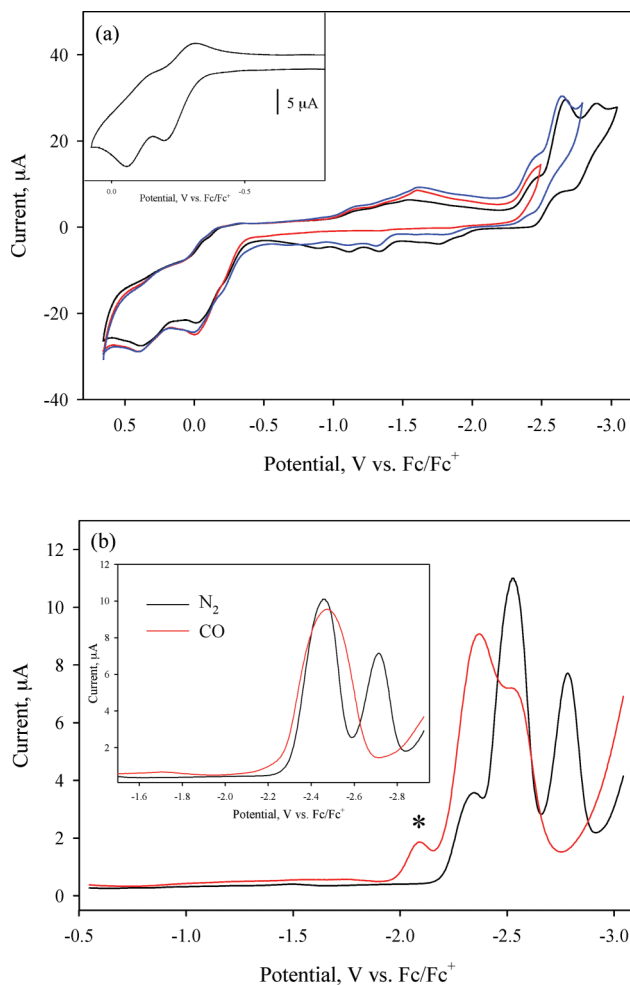
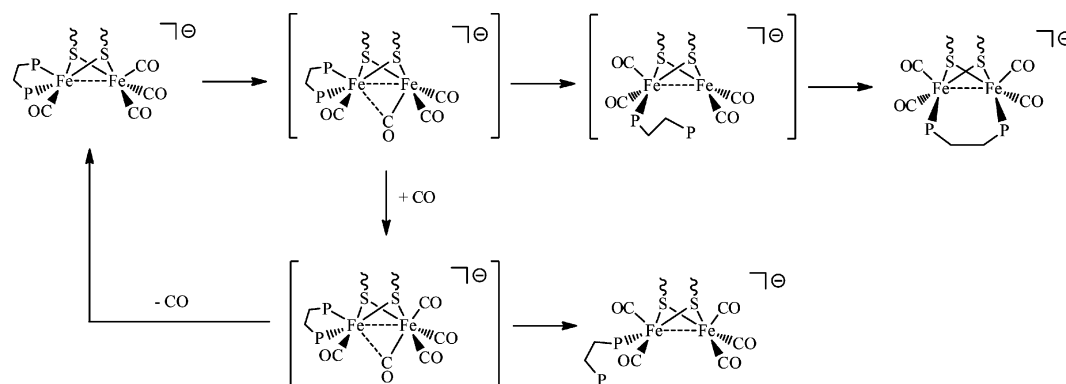


Fig. 9 (a) Cyclic voltammograms of **1** (1 mM) in THF under N_2 ($\nu = 100 \text{ mV s}^{-1}$, 0.1 M $n\text{Bu}_4\text{NPF}_6$, vitreous carbon electrode). The inset shows the voltammogram of **1** recorded in CH_2Cl_2 under the same conditions. (b) Differential pulse voltammograms of **1** in THF under N_2 and CO (amplitude = 50 mV, sample width = 16.7 ms, pulse width = 50 ms, pulse period = 200 ms). The redox wave marked as an asterisk is attributed to the reduction event of the pendant species. The inset shows DPVs of **6** under the same experimental conditions.

the selected metric data are included in the figure caption. Results of electrochemical studies of **6** and **8** confirm the two reduction responses of the κ^2 -complexes in the more negative potential region (-2.64 and -2.80 V for **1**; -2.60 and -2.74 V for **3**) are originated from their μ -isomers. Their oxidation waves are also observed in



Scheme 7

the voltammograms of the κ^2 -species. The responses at 0.28 and 0.38 V are ascribed to oxidations of **6** and the one at 0.35 V to **8**.

The voltammograms recorded under CO provide evidences to further differentiate the events at -2.64 and -2.60 V corresponding to the reduction of **6** and **8**, respectively, and at -2.80 and -2.74 V to the products due to decomposition of the reduced μ -species. Fig. 9b shows voltammetric changes of **1** and **6** recorded by differential pulse technique. The reduction responses at the most negative potential are inhibited by CO purge, referring to that CO dissociation occurs upon reduction of the μ -species. To bear in mind, other chemical reactions are possibly involved such as Fe–S bond cleavage. Since the redox process of the decomposed species is quasi-reversible at electrochemical timescale, electron transfer to the μ -complex triggers formation of one stable product that is yet unknown at this moment. It is postulated any species analogous to the reduction products of $[\text{Fe}_2(\mu\text{-xdt})(\text{CO})_6]$ (xdt = pdt, adt) are generated.³⁷

Transformation of the κ^2 -complex to the corresponding μ -isomer is suppressed upon CO exposure along with appearance of a new species marked as an asterisk in Fig. 9b. Various experimental and theoretical studies have shown that the rotated geometry is favored in the asymmetrically disubstituted $[\text{Fe}_2(\mu\text{-SS})(\text{CO})_4\text{L}_2]$ complexes in which one apical CO group lies underneath the Fe–Fe vector to form the CO bridge or semi-bridge. This assists the CO migration and one coordination site is opened up in such transient species, which is available for exogenous CO-binding. On the other hand, CO dissociation occurs in the reduced state.³⁸ It is not known whether these two CO events proceed consecutively or concomitantly; either regenerates the parent κ^2 -species. This mechanism can explain why isomerization is hindered in the CO atmosphere (Scheme 7). If CO migration occurs instead of CO liberation, the pendant species is formed. Reduction of $[\text{Fe}_2(\mu\text{-S}(\text{CH}_2)_2\text{X}(\text{CH}_2)_2\text{S})(\text{CO})_5\text{L}_2]$ has been recorded at ca. -2.10 V.²⁸ For instance, $(\mu\text{-dppe})[\text{Fe}_2(\mu\text{-S}(\text{CH}_2)_2\text{N}^i\text{Pr}(\text{CH}_2)_2\text{S})(\text{CO})_5]_2$, **2**, is reduced at -2.15 V. Consequently, the minor response at -2.09 and -2.12 V during reduction of **1** and **3**, respectively, under CO is assigned to $[\text{Fe}_2(\mu\text{-S}(\text{CH}_2)_2\text{X}(\text{CH}_2)_2\text{S})(\text{CO})_5(\kappa^1\text{-dppe})]_2$.

In contrast to its μ -isomer, reversibility of the two oxidation waves is conserved for the κ^2 -complex in CH_2Cl_2 . For **3**, they are fully reversible ($i_p^c/i_p^a = 1$), shown in Fig. 10a. These oxidation events are assigned to the $\text{Fe}^{\text{I}}\text{Fe}^{\text{I}}/\text{Fe}^{\text{II}}\text{Fe}^{\text{I}}$ and $\text{Fe}^{\text{II}}\text{Fe}^{\text{I}}/\text{Fe}^{\text{II}}\text{Fe}^{\text{II}}$ redox pairs. The $\Delta E_{1/2}$ difference for the first and second oxidation processes of 170 mV indicates weak electronic communication be-

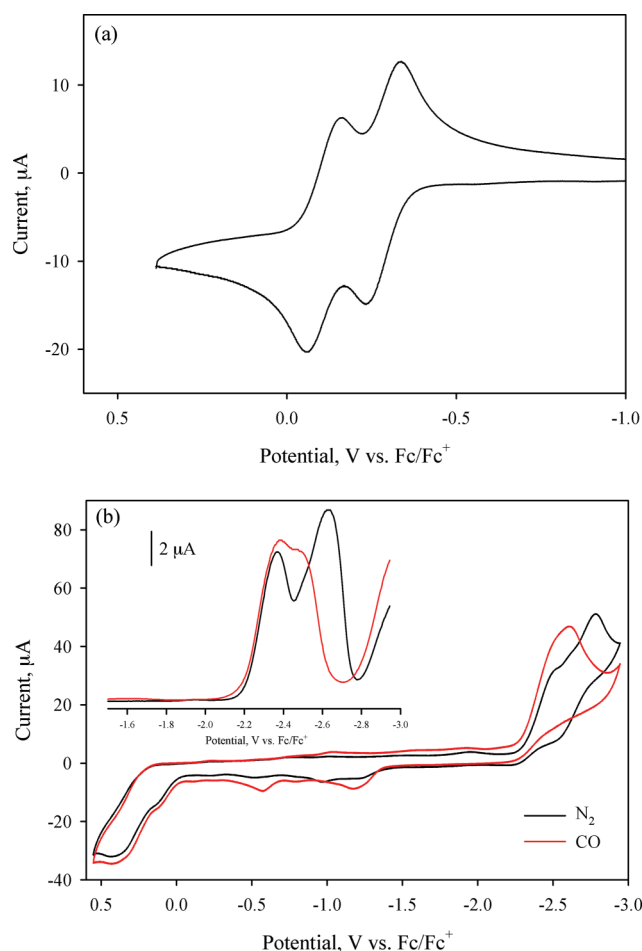


Fig. 10 (a) Cyclic voltammogram of **3** (1 mM) in CH_2Cl_2 ($v = 100 \text{ mV s}^{-1}$, 0.1 M $n\text{-Bu}_4\text{NPF}_6$, vitreous carbon electrode) under N_2 , showing two successive reversible two-electron transfer events. (b) Cyclic voltammograms of **7** (1 mM) in THF ($v = 100 \text{ mV s}^{-1}$, 0.1 M $n\text{-Bu}_4\text{NPF}_6$, vitreous carbon electrode) under N_2 and CO. The inset shows the changes of differential pulse voltammograms of **7** (amplitude = 50 mV, sample width = 16.7 ms, pulse width = 50 ms, pulse period = 200 ms).

tween the two Fe centers. A comproportionation constant (K_{comp}) of 752 was calculated according to $\Delta E_{1/2} (\text{V}) = 0.0591(\log K_{\text{comp}})$. This suggests that removal of electrons takes place from almost electronically discrete redox levels. The metal–metal distances of

complexes **1** and **3** (2.541 and 2.549 Å) are comparable to those of the known species (2.53–2.57 Å), in which mixed-valence states are isolated.^{18–20} Theoretical calculations have shown that the HOMO is predominately from Fe contributions. Thus factors other than d-d overlap are possible origins for the existence of mixed-valence Fe^{II}Fe^I complexes.³⁹ Likewise, two reductions of complex **7** are better resolved than for its dppe counterpart under the same experimental conditions, as displayed in Fig. 10b. Contributions of ligand field due to structural distortion should not be negligible. Management of electronic structure and electron transfer within the Fe centers *via* tuning the ligand field is essential to understanding of catalytic property of the model complexes. Further studies are currently under investigation.

Concluding remarks

Factors that are in control of the distortion within the [Fe₂] units are discussed in this report. In addition to electronic asymmetry, the results indicate the intramolecular N...C(CO_{ap}) interaction plays a crucial role on rotation of the Fe(CO)₃ moiety. Fig. 11 displays an almost eclipsed configuration within complex **1** is observed in the presence of the interaction. In contrast, a significant twist is formed upon removal of the interaction from availability of the aza nitrogen lone pairs. The distortion angles of 34.1 and 35.4° (av.) for complexes **4** and **5**, respectively, are the largest among their class.

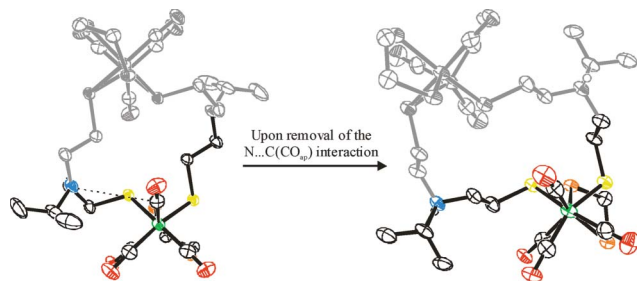


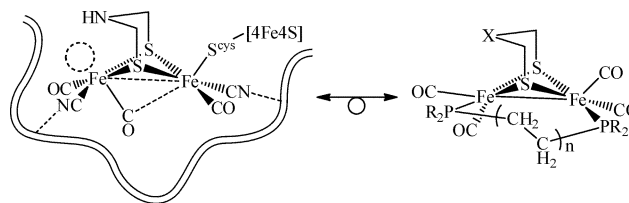
Fig. 11 Presentation of the distortion along the Fe–Fe axis upon removal of the N...C(CO_{ap}) interaction within **1** *via* protonation/methylation of the aza nitrogen sites. Only the partial molecules are highlighted for a clearer view.

The κ²-mode coordination of dppe in complex **1** generates the electron richer Fe(CO)P₂ and the more electron deficient Fe(CO)₃ moieties. Electronic inequivalence is attested by the substantially shorter distance between the aza nitrogen and the apical carbonyl carbon of the Fe(CO)₃ moiety, 3.796(4) Å, compared to that of 4.011(3) Å in the all-CO molecule.

Different degrees of distortion are also caused by the bridging diphosphines. A larger ϕ angle of 26.5° for **6** is probably resulted from the least strained structure with the bridge of dppe to two Fe centers. On the contrary, the short backbone of dppm does not allow any substantial twist but a compact structure of **7** with ϕ = 3.9° (av.).

In reality, the active site of Fe-only hydrogenase is encapsulated inside the protein pocket wherein hydrogen bonds between the bound CN⁻ ligands and the peptide chain are present.^{7,40} The peptide backbone that is in control of the rotated geometry of the active site *via* hydrogen bonding would slightly modulate the twist as morphology of the protein changes to adopt the

optimal stereoisomer for catalysis. The bridging diphosphines with an appropriate length within the [Fe₂(μ-xdt)(CO)₄P₂] unit well resemble a combination of CN⁻ ligands and the peptide chain as the donor ends and the chain backbone are already present. For the donor ability this can be tuned by different substituents on the phosphines. However, modulation of electron richness about the Fe centers *via* hydrogen bonding is a dynamic process in proteins. This will be a challenge for synthetic chemists to overcome.



Experimental section

General methods

All reactions were carried out by using standard Schlenk and vacuum-line techniques under an atmosphere of purified nitrogen. All commercial available chemicals were of ACS grade and used without further purification. Solvents were of HPLC grade and purified as follows: diethyl ether and THF were distilled from sodium/benzophenone under N₂. Hexane was distilled from sodium under N₂. Dichloromethane was distilled from CaH₂ under N₂. Acetonitrile was distilled first over CaH₂ and then from P₂O₅ under N₂. Deuterated solvents obtained from Merck were distilled over 4 Å molecular sieves under N₂ prior to use. Preparation of [Fe₂(μ-S(CH₂)₂NⁱPr(CH₂)₂S)(CO)₆]₂, [Fe₂(μ-S(CH₂)₂S)(CO)₆]₂ and ⁱPrN(CH₂CH₂SH)₂ was previously described.⁴¹

Infrared spectra were recorded on a Perkin Elmer Spectrum One using a 0.05-mm CaF₂ cell. ¹H, ¹³C{¹H} and ³¹P{¹H} NMR spectra were recorded on a Bruker AV-500 or DRX-500 spectrometer operating at 500, 125.7 and 202.49 MHz, respectively. Spectra are referenced to tetramethylsilane (TMS) for ¹H and ¹³C{¹H}, and 85% H₃PO₄ for ³¹P{¹H} NMR spectra. Mass spectral analyses were done on a Waters LCT Premier XE at Mass Spectrometry Center in the Institute of Chemistry, Academia Sinica. Elemental analyses were performed on an Elementar vario EL III elemental analyzer.

Electrochemistry

Electrochemical measurements were recorded on a CH Instruments 630 C electrochemical potentiostat using a gastight three-electrode cell under N₂ at room temperature or at the specific temperature mentioned. A glassy carbon electrode and a platinum wire were used as working and auxiliary electrodes, respectively. Reference electrode was a non-aqueous Ag/Ag⁺ electrode (0.01 M AgNO₃/0.1 M ⁿBu₄NPF₆). All potentials are measured in 0.1 M ⁿBu₄NPF₆ solution in CH₂Cl₂ or THF. They are reported against ferrocene/ferrocenium (Fc/Fc⁺). Controlled-potential electrolysis of complexes **1** and **3** was performed at the working potential 100 mV more negative than the corresponding first reduction event in order not to exceed the reduction potential of the μ-isomer.

Table 4 X-Ray crystallographic data

	1·2CH ₂ Cl ₂	2·2CH ₂ Cl ₂	3	[4](TFA) ₂ ·4CH ₂ Cl ₂ · 2O(CH ₂ CH ₃) ₂	[5](OTf) ₂ ·1.5CH ₂ Cl ₂ · O(CH ₂ CH ₃) ₂ · 2CH ₃ CN	6·THF	7·4THF
Empirical formula	C ₇₆ H ₈₂ Cl ₄ Fe ₄ - N ₂ O ₈ P ₄ S ₄	C ₅₂ H ₅₈ Cl ₄ Fe ₄ - N ₂ O ₁₀ P ₂ S ₄	C ₇₀ H ₆₈ Fe ₄ O ₈ - P ₄ S ₄	C ₉₀ H ₁₀₈ Cl ₈ F ₆ Fe ₄ - N ₂ O ₁₄ P ₄ S ₄	C _{87.5} H ₁₀₃ Cl ₃ F ₆ - Fe ₄ N ₄ O ₁₅ P ₄ S ₆	C ₇₈ H ₈₆ Fe ₄ - N ₂ O ₆ P ₄ S ₄	C ₈₈ H ₁₀₆ Fe ₄ - N ₂ O ₁₂ P ₄ S ₄
<i>M_r</i>	1768.76	1426.38	1512.76	2314.90	2210.73	1671.01	1859.27
<i>T</i> /K	150(2)	150(2)	150(2)	150(2)	150(2)	150(2)	150(2) K
Crystal system	Monoclinic	Monoclinic	Triclinic	Monoclinic	Triclinic	Tetragonal	Monoclinic
Space group	<i>P</i> 2 ₁ / <i>n</i>	<i>P</i> 2 ₁ / <i>n</i>	<i>P</i> $\bar{1}$	<i>P</i> 2 ₁ / <i>n</i>	<i>P</i> $\bar{1}$	<i>P</i> 4 ₂ /2	<i>C</i> <i>c</i>
<i>a</i> /Å	15.7127(2)	13.2880(6)	10.63200(10)	17.133(3)	16.4839(5)	15.5258(4)	37.7214(7)
<i>b</i> /Å	13.9213(2)	21.5592(9)	17.8511(2)	13.281(2)	17.0452(5)	15.5258(4)	13.5805(3)
<i>c</i> /Å	18.6454(3)	21.8668(9)	20.8444(2)	23.904(4)	21.2654(4)	33.5050(8)	21.1039(4)
α /°	90	90	110.0752(6)	90	94.2320(2)	90	90
β /°	94.2687(7)	102.760(1)	96.6827(6)	107.252(8)	108.7318(14)	90	123.2606(12)
γ /°	90	90	106.1587(6)	90	113.5410(11)	90	90
<i>V</i> /Å ³	4067.20(10)	6109.7(5)	3469.11(6)	5194.5(15)	5045.1(2)	8076.4(4)	9040.0(3)
<i>Z</i>	2	4	2	2	2	4	4
<i>D_c</i> /Mg m ⁻³	1.444	1.551	1.448	1.480	1.455	1.374	1.366
μ /mm ⁻¹	1.065	1.350	1.086	0.965	0.903	0.942	0.851
<i>F</i> (000)	1824	2920	1560	2384	2282	3472	3888
Reflections collected	23077	46682	42631	20998	63604	27175	30121
Independent reflections	9311	14029	15859	9021	17651	9224	18044
<i>R</i> _{int}	0.0452	0.0489	0.0338	0.0997	0.0917	0.0442	0.0508
Goodness-of-fit on <i>F</i> ²	1.001	1.068	1.017	1.031	1.008	1.068	1.030
<i>R</i> ₁ [<i>I</i> > 2σ(<i>I</i>)] (all data) ^a	0.0445 (0.0772)	0.0557 (0.0722)	0.0322 (0.0491)	0.0920 (0.1806)	0.1006 (0.1789)	0.0487 (0.0706)	0.0511 (0.0862)
w <i>R</i> ₂ [<i>I</i> > 2σ(<i>I</i>)] (all data) ^b	0.1119 (0.1254)	0.1287 (0.1380)	0.0749 (0.0825)	0.2289 (0.2928)	0.2871 (0.3409)	0.1344 (0.1466)	0.1119 (0.1279)

$$^a R_1 = (\sum \|F_o\| - |F_c|) / (\sum |F_o|). \quad ^b wR_2 = [\sum w(F_o^2 - F_c^2)^2 / \sum w(F_o^2)^2]^{1/2}.$$

Molecular structure determinations

The X-ray single crystal crystallographic data collections for **1–7** were carried out at 150 K on a Bruker SMART APEX CCD four-circle diffractometer with graphite-monochromated Mo-*K*α radiation ($\lambda = 0.71073$ Å) outfitted with a low-temperature, nitrogen-stream aperture. The structures were solved using direct methods, in conjunction with standard difference Fourier techniques and refined by full-matrix least-squares procedures. A summary of the crystallographic data for complexes **1–7** is shown in Table 4. An empirical absorption correction (multi-scan) was applied to the diffraction data for all structures. All non-hydrogen atoms were refined anisotropically and all hydrogen atoms were placed in geometrically calculated positions by the riding model. All software used for diffraction data processing and crystal structure solution and refinement are contained in the SHELXL-97 program suites.⁴² The X-ray data refinement *R*₁ = 0.092 of complex **4** was improved to 0.0759 after removal of co-crystallized solvents by the SQUEEZE function in the SHELXL program. A similar refinement was operated for complex **5**. The X-ray data refinement *R*₁ = 0.1006 was improved to 0.0791. A summary of the crystallographic data for complexes **4** and **5** after the SQUEEZE refinement is shown in Table S1 (ESI†).

Synthesis of [Fe₂(μ-S(CH₂)₂NⁱPr(CH₂)₂S)(CO)₄(κ²-dppe)]₂, **1**, and (μ-dppe)[Fe₂(μ-S(CH₂)₂NⁱPr(CH₂)₂S)(CO)₅]₂, **2**

A solution of [Fe₂(μ-S(CH₂)₂NⁱPr(CH₂)₂S)(CO)₆]₂ (500 mg, 0.55 mmol) and dppe (800 mg, 2 mmol) in 17 mL of toluene was heated at 90 °C for 6 h. The precipitate was settled and the red solution was transferred to a different flask. The dark green powder was then washed with toluene a few times until the upper

solution is almost clear. [Fe₂(μ-S(CH₂)₂NⁱPr(CH₂)₂S)(CO)₄(κ²-dppe)]₂, **1**, was obtained as a dark green solid in 60% yield (524 mg). Crystals of [Fe₂(μ-S(CH₂)₂NⁱPr(CH₂)₂S)(CO)₄(κ²-dppe)]₂·2CH₂Cl₂ suitable for X-ray crystallographic analysis were grown from the CH₂Cl₂–MeOH solution at –20 °C. The red extract was dried under vacuum and purified by chromatography on silica gel with CH₂Cl₂ as the eluent. The red band, **2**, was obtained as a red solid in 21% yield (143 mg). Crystals of (μ-dppe)[Fe₂(μ-S(CH₂)₂NⁱPr(CH₂)₂S)(CO)₅]₂·2CH₂Cl₂ suitable for X-ray crystallographic analysis were grown from the CH₂Cl₂–MeOH solution at –20 °C. **1**: IR (CH₂Cl₂, cm⁻¹): ν_{CO} 2016 (vs), 1944 (vs), 1895 (w). ¹H NMR (500 MHz, CD₂Cl₂, 253 K): 0.69 (d, ³J_{HH} = 6 Hz, 6H, 2 CH₃), 0.75 (d, ³J_{HH} = 6 Hz, 6H, 2 CH₃), 1.74 (t, 2H, 1 CH₂), 2.09 (m, 6H, 3 CH₂), 2.35 (m, 4H, 1 CH₂ + 2 NCH), 2.46 (m, 3H, 2 CH₂), 2.64 (m, 7H, 4 CH₂), 2.80 (m, 4H, 2 CH₂), 7.05–7.88 (m, 40H, 8 Ph) ppm. ¹³C{¹H} NMR (125.7 MHz, CD₂Cl₂, 253 K): 19.44 (2 CH₃), 20.12 (1 CH₂), 20.57 (2 CH₃), 29.14 (2 CH₂), 36.44 (2 CH₂), 51.23 (2 CH₂), ~54 (CH₂ + 2 NCH, overlapped with d-solvent), 127.69, 128.80, 129.20, 129.84, 130.56, 131.80, 132.58, 133.79, 134.99, 137.43 (8 Ph), 213.71 (CO) ppm. ³¹P{¹H} NMR (202.48 MHz, CD₂Cl₂, 253 K): 83.23 (d, *J*_{PP} = 12.8 Hz, 2P), 85.47 (d, *J*_{PP} = 12.8 Hz, 2P) ppm. ESI-MS: *m/z* 1599.95 {**1** + H⁺}⁺. Anal. Calc. for C₇₄H₇₈Fe₂N₂O₈P₄S₄: C, 55.59; H, 4.92; N, 1.75. Found: C, 55.37; H, 4.93; N, 1.74. **2**: IR (CH₂Cl₂, cm⁻¹): ν_{CO} 2041 (vs), 1985 (vs), 1971 (sh), 1960 (sh), 1929 (w). ¹H NMR (500 MHz, CD₂Cl₂, 243 K): 0.71 (d, ³J_{HH} = 6 Hz, 6H, 2 CH₃), 1.09 (d, ³J_{HH} = 6 Hz, 6H, 2 CH₃), 1.41 (b, 2H, 1 CH₂), 1.66 (m, 3H, 2 CH₂), 2.08 (m, 4H, 2 CH₂), 2.50 (m, 2H, 1 CH₂), 2.58 (m, 4H, 2 CH₂ + 1 NCH), 2.87 (m, 4H, 2 CH₂), 3.10 (m, 3H, 1 CH₂ + 1 NCH), 7.41–7.67 (m, 20H, 4 Ph) ppm. ¹³C{¹H} NMR (125.7 MHz, CD₂Cl₂, 243 K): 19.09 (4 CH₃), 26.55 (2 CH₂), 28.11 (2 CH₂), 40.51 (2 CH₂), ~54 (2 CH₂, overlapped with d-solvent),

55.4 (1 NCH), 56.15 (1 NCH), 56.27 (2 CH₂), 129.23, 129.40, 129.55, 129.65, 129.95, 130.17, 130.42, 130.93, 131.57, 132.45, 133.90, 136.11 (4 Ph), 211.10, 213.61, 213.89, 215.40 (CO) ppm. ³¹P{¹H} NMR (202.48 MHz, CD₂Cl₂, 243 K): 54.14 ppm; (298 K): 54.91, 58.36 ppm. ESI-MS: *m/z* 1256.92 {**2** + H⁺}⁺. Anal. Calc. for C₅₀H₅₄Fe₄N₂O₁₀P₂S₄: C, 47.79; H, 4.33; N, 2.23. Found: C, 47.74; H, 4.35; N, 2.23%.

Synthesis of [Fe₂(μ-S(CH₂)₅S)(CO)₄(κ²-dppe)]₂, **3**

To a flask containing 185 mg (0.22 mmol) of [Fe₂(μ-S(CH₂)₅S)(CO)₆]₂ and 312 mg (0.78 mmol) of dppe was added 6 mL of toluene. The flask was transferred to an oil-bath and heated at 90 °C for 8 h. The upper solution was removed *via* cannula. The green solid was washed by at least three portions of 4 mL of toluene until the upper solution was almost clear. The solid was dried under vacuum and re-dissolved in CH₂Cl₂. The green powder was precipitated upon the addition of hexane to the CH₂Cl₂ solution. The green product was dried and its yield was calculated to 59% (199.5 mg). Crystals suitable for X-ray crystallographic analysis of [Fe₂(μ-S(CH₂)₅S)(CO)₄(κ²-dppe)]₂ were grown from the CH₂Cl₂ solution layered with methanol at -20 °C. IR (CH₂Cl₂, cm⁻¹): ν_{CO} 2017 (vs), 1943 (vs), 1894 (w). ¹H NMR (500 MHz, CD₂Cl₂, 263 K): 0.10 (t, *J* = 12 Hz, 2H, 1 CH₂), 0.85 (m, 4H, 2 CH₂), 0.92 (m, 2H, 1 CH₂), 1.55 (m, 2H, 1 SCH₂), 1.76 (m, 2H, 1 SCH₂), 1.91 (m, 2H, 1 CH₂), 2.02 (m, 2H, 1 CH₂), 2.15 (m, 2H, 1 SCH₂), 2.31 (m, 2H, 1 SCH₂), 2.70 (m, 6H, 3 PCH₂), 2.87 (m, 2H, 1 PCH₂), 7.03–7.92 (m, 40H, 8 Ph) ppm. ¹³C{¹H} NMR (125.7 MHz, CD₂Cl₂, 263 K): 22.87 (2 CH₂), 25.68 (1 CH₂), 29.13 (d, *J*_{PC} = 11.3 Hz, 1 PCH₂), 29.35 (d, *J*_{PC} = 11.3 Hz, 1 PCH₂), 30.02 (2 CH₂), 31.02 (1 CH₂), 31.36 (d, *J*_{PC} = 15.6 Hz, 1 PCH₂), 31.58 (d, *J*_{PC} = 15.6 Hz, 1 PCH₂), 32.10 (2 SCH₂), 38.10 (2 SCH₂), 127.79, 127.73, 128.75, 128.82, 129.23, 129.71, 129.91, 130.61, 131.91, 131.99, 132.08, 132.91, 132.96, 133.92, 133.99, 134.95, 135.05, 135.18, 135.37, 138.15, 138.36, 138.50, 138.80 (8 Ph), 213.95 (6 CO), 218.07 (CO), 218.28 (CO) ppm. ³¹P{¹H} NMR (202.48 MHz, CD₂Cl₂, 263 K): 84.43 (d, *J*_{PP} = 14.6 Hz, 2P), 85.34 (d, *J*_{PP} = 14.6 Hz, 2P) ppm. FAB+MS: *m/z* 1514.03 {**3** + H⁺}⁺. Anal. Calc. for C₇₀H₆₈Fe₄O₈P₄S₄: C, 55.57; H, 4.53. Found: C, 55.14; H, 4.52%.

Synthesis of [Fe₂(μ-S(CH₂)₂NⁱPr(H)(CH₂)₂S)(CO)₄(κ²-dppe)]₂(TFA)₂, **[4](TFA)**₂

A solution of 100 mg (0.063 mmol) of **1** in 5 mL of CH₂Cl₂ was treated with 14 μL (0.19 mmol) of TFA. After it was stirred for 20 min, the solution was dried under vacuum. The dark brown residue was washed by 30 mL of ether three times and was re-dissolved in 3 mL of CH₂Cl₂. The product was precipitated as a dark green powder upon the addition of 30 mL of hexane. The product was collected and dried under vacuum in 80% yield (92 mg) after the upper solution was removed. Crystals of [Fe₂(μ-S(CH₂)₂NⁱPr(H)(CH₂)₂S)(CO)₄(κ²-dppe)]₂(CF₃CO₂)₂·4CH₂Cl₂·2O(CH₂CH₃)₂ suitable for X-ray crystallographic analysis were grown from the CH₂Cl₂ solution layered with ether at -20 °C. IR (CH₂Cl₂, cm⁻¹): ν_{CO} 2024 (vs), 1958 (vs), 1945 (vs), 1904 (w); ν_{COO} 1684 (w), 1671 (w). ¹H NMR (500 MHz, CD₂Cl₂, 298 K): 0.75 (d, ³*J*_{HH} = 5 Hz, 6H, 2 CH₃), 0.83 (d, ³*J*_{HH} = 5 Hz, 6H, 2 CH₃), 0.87–1.28 (m, 8H, 4 CH₂), 1.94 (t, 1H, 1 CH₂),

2.41–3.35 (m, 17H, 2 NCH + 8 CH₂), 7.82, 7.87 (br, 2H, 2NH), 6.93–7.99 (m, 40H, 8 Ph) ppm. ³¹P{¹H} NMR (202.48 MHz, CD₂Cl₂, 225 K): 81.89 (2P), 84.33 (2P) ppm. ESI-MS: *m/z* 1713.06 {[**4**](TFA)}⁺, 1598.99 {**4** - H⁺}⁺, 1487.17 {**4** - 4CO - H⁺}⁺. Anal. Calc. for C₇₈H₈₀F₆Fe₄N₂O₁₂P₄S₄: C, 51.28; H, 4.41; N, 1.53. Found: C, 50.87; H, 4.43; N, 1.53%.

Synthesis of [Fe₂(μ-S(CH₂)₂NⁱPr(Me)(CH₂)₂S)(CO)₄(κ²-dppe)]₂(OTf)₂, **[5](OTf)**₂

A solution of 174 mg (0.11 mmol) of **1** in 8 mL of CH₂Cl₂ was treated with 120 μL (1.1 mmol) MeOTf. After it was stirred for 1 h at room temperature, the solution was dried under vacuum. The brick-red residue was washed by 20 mL of ether twice. The brick-red powder was precipitated from the CH₂Cl₂ solution upon the addition of excess hexane. The product was collected and dried under vacuum in 96% yield (203 mg) after the upper solution was removed. Crystals of [Fe₂(μ-S(CH₂)₂NⁱPr(Me)(CH₂)₂S)(CO)₄(κ²-dppe)]₂(OTf)₂·1.5CH₂Cl₂·O(CH₂CH₃)₂·2CH₃CN suitable for X-ray crystallographic analysis were grown from the CH₃CN-CH₂Cl₂ mixed solution layered with ether at -20 °C. IR (CH₂Cl₂, cm⁻¹): ν_{CO} 2026 (vs), 1961 (vs), 1940 (vs), 1907 (w). ¹H NMR (500 MHz, CD₂Cl₂, 253 K): 0.65–1.47 (m, 20H, 4 CH₃ + 4 CH₂), 1.71–3.9 (m, 24H, 8 CH₂ + 2 NCH₃ + 2 NCH), 6.78–7.94 (m, 40H, 8 Ph) ppm. ³¹P{¹H} NMR (202.48 MHz, CD₂Cl₂, 225 K): 83.39 (2P), 80.44 (2P) ppm. ESI-MS: *m/z* 1777.1 {[**5**](OTf)}⁺, 814.1 {[**5**]}²⁺. Anal. Calc. for C₇₉H₈₆F₆Fe₄N₂O₁₄P₄S₆Cl₂: C, 47.16; H, 4.31; N, 1.39. Found: C, 47.03; H, 4.54; N, 1.48%.

Electrosynthesis of [Fe₂(μ-S(CH₂)₂NⁱPr(CH₂)₂S)(μ-dppe)(CO)]₂, **6**

30 mL of THF was added to an electrochemical cell containing 70 mg (0.044 mmol) of **1** and 1.16 g (3 mmol) of ⁿBu₄NPF₆. Graphite rods (6.15 mm in diameter) were used as working and auxiliary electrodes. The reference electrode was a non-aqueous Ag/Ag⁺ electrode. The working potential was set to -2.54 V. The solution was monitored by *in situ* FTIR spectroscopy (Mettler Toledo ReactIR iC10 equipped with a MCT detector and a 0.625-inch SiComp probe) throughout bulk electrolysis. The IR signatures of **1** decreased as those of **6** increased. The electrolysis experiment was stopped when the IR bands of **1** disappeared. The charge passage of 1.57 C (0.37 F mol⁻¹ of **1**) was recorded. The solution was then transferred to a Schlenk flask *via* cannula and dried under vacuum to obtain a red-brown solid. Three portions of 30 mL of ether were used to extract the product from the mixture containing the electrolyte. The extract was purified by column chromatography on silica gel with CH₂Cl₂ as the eluent to remove free dppe ligand and then with CH₂Cl₂-ethyl acetate-hexane (v/v/v 1/1/2) to obtain a red-brown band. The yield of **6** is 70% (49 mg). Crystals of [Fe₂(μ-S(CH₂)₂NⁱPr(CH₂)₂S)(μ-dppe)(CO)]₂·THF suitable for X-ray crystallographic analysis were grown from a THF solution layered with hexane at -20 °C. IR (CH₂Cl₂, cm⁻¹): ν_{CO} 1982 (m), 1954 (vs), 1914 (s), 1891 (w). ¹H NMR (500 MHz, CD₂Cl₂, 253 K): 0.95 (m, 4H, 2 CH₂), 1.01 (d, ³*J*_{HH} = 6 Hz, 12H, 4 CH₃), 1.80 (m, 2H, 1 CH₂), 2.24 (b, 4H, 2 CH₂), 2.62 (t, ³*J*_{HH} = 8 Hz, 4H, 2 CH₂), 2.78 (b, 6H, 2 CH₂ + 2 NCH), 2.91 (b, 4H, 2 CH₂), 3.66 (m, 2H, 1 CH₂), 7.31–7.75 (m, 40H, 8 Ph) ppm. ¹³C{¹H} NMR (125.7 MHz, CD₂Cl₂, 253 K): 18.46 (4 CH₃ + 2 CH₂), 26.04 (1 CH₂), 27.85 (2 CH₂), 39.02 (2 CH₂), 51.17 (2 CH₂),

51.98 (2 NCH), 53.47 (2 CH₂), 68.26 (1 CH₂), 128.43, 128.51, 128.98, 129.05, 129.91, 130.58, 130.90, 130.94, 134.20, 134.26 (8 Ph), 215.35, 215.40, 217.42, 217.60 (CO) ppm. ³¹P{¹H} NMR (202.48 MHz, CD₂Cl₂, 233 K): 55.57, 66.48 ppm. ESI-MS: *m/z* 1599.04 {**6** + H⁺}⁺, 1487.16 {**6** - 4CO + H⁺}⁺. Anal. Calc. for C₇₄H₇₈Fe₄N₂O₈P₄S₄: C, 55.59; H, 4.92; N, 1.75. Found: C, 55.89; H, 5.07; N, 1.79%.

Synthesis of [Fe₂(μ-S(CH₂)₂NⁱPr(CH₂)₂S)(μ-dppm)(CO)₄]₂, **7**

To a flask containing 300 mg (0.33 mmol) of **1** and 290 mg (0.75 mmol) of dppm was added 15 mL of toluene. The flask was transferred to an oil-bath and heated at 105 °C for 19 h. The solution was then refluxed for 5 h to complete the reaction. The solution was dried under vacuum to afford a red solid. It was purified by chromatography on silica gel with CH₂Cl₂ as the eluent to remove free dppm and then CH₂Cl₂-diethyl ether (v/v 6/1) to obtain the product, **7**, as a red band. It was dried under reduced pressure to afford a red solid in 88% yield (454 mg). Crystals of [Fe₂(μ-S(CH₂)₂NⁱPr(CH₂)₂S)(μ-dppm)(CO)₄]₂·4THF suitable for X-ray crystallographic analysis were grown from THF-hexane solution at -20 °C. IR (CH₂Cl₂, cm⁻¹): ν_{CO} 1982 (m), 1958 (vs), 1916 (s), 1899 (sh). ¹H NMR (500 MHz, CD₂Cl₂, 253 K): 0.96 (d, ³J_{HH} = 6.5 Hz, 12H, 4 CH₃), 2.44 (t, ³J_{HH} = 7.5 Hz, 4H, 2 CH₂), 2.50 (b, 4H, 2 CH₂), 2.66 (t, ³J_{HH} = 8.0 Hz, 4H, 2 CH₂), 2.80 (m, 4H, 2 CH₂ + 2 NCH), 3.41 (dt, *J* = 14, 11 Hz, 2H, PCH₂P), 4.03 (dt, *J* = 14, 11 Hz, 2H, PCH₂P), 7.29–7.61 (m, 40H, 8 Ph) ppm. ¹³C{¹H} NMR (125.7 MHz, CD₂Cl₂, 253 K): 18.57 (4 CH₃), 23.93 (2 CH₂), 39.07 (2 CH₂), 39.96 (t, *J* = 21.8 Hz, 2 PCH₂P), 51.43 (2 CH₂), 52.01 (2 NCH), 52.98 (2 CH₂), 128.47, 128.85, 130.18, 130.30, 131.92, 131.96, 131.99, 132.75, 132.79 (8 Ph), 215.32 (CO), 219.01 (d, *J* = 10.7 Hz, CO), 219.10 (d, *J* = 10.7 Hz, CO) ppm. ³¹P{¹H} NMR (202.48 MHz, CD₂Cl₂, 253 K): 51.18 (s) ppm. ESI-MS: *m/z* 1570.98 {**7** + H⁺}⁺. Anal. Calc. for C₇₆H₈₂Fe₄N₂O₉P₄S₄: C, 55.56; H, 5.03; N, 1.71. Found: C, 55.58; H, 5.32; N, 1.66%.

Electrosynthesis of [Fe₂(μ-S(CH₂)₅S)(μ-dppe)(CO)₄]₂, **8**

The similar procedure to synthesis of complex **6** was applied to preparation of complex **8**. The working potential was set to -2.46 V. The charge passage of 0.96 F mol⁻¹ of **3** was recorded. The yield of **8** as a red solid is 90%. IR (CH₂Cl₂, cm⁻¹): ν_{CO} 1983 (m), 1955 (vs), 1917 (s), 1898 (w). ¹H NMR (500 MHz, CD₂Cl₂, 298 K): 1.54 (m, 2H, CH₂), 1.71 (m, 8H, 4 CH₂), 2.11 (m, 2H, CH₂), 2.36 (m, 4H, 2 CH₂), 2.45–2.53 (m, 12H, 6 CH₂), 7.35–7.79 (m, 40H, 8 Ph) ppm. ¹³C{¹H} NMR (125.7 MHz, CD₂Cl₂, 298 K): 24.24 (4 CH₃), 25.44 (1 CH₂), 26.08 (2 CH₂), 27.41 (1 CH₂), 29.84 (1 CH₂), 30.20 (1 CH₂), 31.24 (1 CH₂), 32.74 (1 CH₂), 36.11 (1 CH₂), 37.99 (1 CH₂), 128.36, 128.43, 128.86, 128.93, 129.84, 130.31, 131.08, 131.15, 133.84, 133.91, 133.96, 136.31, 136.61, 139.43, 139.77 (8 Ph), 215.22, 215.30, 217.36, 217.55 (CO) ppm. ³¹P{¹H} NMR (202.48 MHz, CD₂Cl₂, 298 K): 60.48 ppm. Anal. Calc. for C₇₀H₆₈Fe₄O₈P₄S₄: C, 55.57; H, 4.53; S, 8.48. Found: C, 55.24; H, 4.52; S, 8.47%.

Reaction of (μ-dppe)[Fe₂(μ-S(CH₂)₂NⁱPr(CH₂)₂S)(CO)₅]₂ and PPh₂Me

To a red solution of 60 mg (0.048 mmol) of complex **2** in 10 mL of toluene was added 9 μL (0.048 mmol) PPh₂Me.

The solution was gently heated at 45 °C and was monitored by FTIR and ³¹P NMR spectroscopy frequently. The solution was dried under reduced pressure once the spectra indicated PPh₂Me was consumed. The solid was re-dissolved in CH₂Cl₂ and was washed by CH₂Cl₂-MeOH several times to obtain a brown solid. [Fe₂(μ-S(CH₂)₂NⁱPr(CH₂)₂S)(CO)₄(κ²-dppe)][Fe₂(μ-S(CH₂)₂NⁱPr(CH₂)₂S)(CO)₅(PPh₂Me)], **9**, was obtained in 75% (51 mg) yield. IR (CH₂Cl₂, cm⁻¹): ν_{CO} 2039 (s), 2015 (m), 1979 (vs), 1949 (vs), 1934 (sh), 1895 (w). ¹H NMR (500 MHz, CD₂Cl₂): 0.71 (m, 6H, 2 CH₃), 0.84 (m, 6H, 2 CH₃), 2.16 (m, 3H, PCH₃), 1.76–2.74 (m, 22H, 10 CH₂ + 2 NCH), 7.06–7.97 (m, 30H, 6 Ph) ppm. ³¹P{¹H} NMR (202.48 MHz, CD₂Cl₂, 296.5 K): 42.89, 86.90 (d, *J*_{PP} = 11 Hz, 1P), 88.97 (d, *J*_{PP} = 11 Hz, 1P); 43.70, 87.57 (d, *J*_{PP} = 11 Hz, 1P), 89.80 (d, *J*_{PP} = 11 Hz, 1P); 43.55, 85.72 (d, *J*_{PP} = 11 Hz, 1P), 86.63 (d, *J*_{PP} = 11 Hz, 1P) ppm in a ratio of 6 : 2 : 1. ESI-MS: *m/z* 1429.03 {**9** + H⁺}⁺.

Acknowledgements

We are grateful to financial support from National Science Council of Taiwan and Academia Sinica. We also thank Drs. Mei-Chun Tseng and Su-Ching Lin for help with MS analysis and 2D NMR experiments, respectively.

References

- (a) M. W. W. Adams and E. I. Stiefel, *Curr. Opin. Chem. Biol.*, 2000, **4**, 214–220; (b) J. C. Fontecilla-Camps, A. Volbeda, C. Cavazza and Y. Nicolet, *Chem. Rev.*, 2007, **107**, 4273–4303; (c) C. Tard and C. J. Pickett, *Chem. Rev.*, 2009, **109**, 2245–2274.
- (a) G. J. Kubas, *Chem. Rev.*, 2007, **107**, 4152–4205; (b) A. L. De Lacey, V. M. Fernández, M. Rousset and R. Cammack, *Chem. Rev.*, 2007, **107**, 4304–4330.
- (a) W.-F. Liaw, W.-T. Tsai, H.-B. Gau, C.-M. Lee, S.-Y. Chou, W.-Y. Chen and G.-H. Lee, *Inorg. Chem.*, 2003, **42**, 2783–2788; (b) C. Tard, X. Liu, S. K. Ibrahim, M. Bruschi, L. De Gioia, S. C. Davies, X. Yang, L.-S. Wang, G. Sawers and C. J. Pickett, *Nature*, 2005, **433**, 610–613; (c) J. D. Lawrence, H. Li and T. B. Rauchfuss, *Chem. Commun.*, 2001, 1482–1483; (d) M. Razavet, S. C. Davies, D. L. Hughes and C. J. Pickett, *Chem. Commun.*, 2001, 847–848; (e) J. W. Tye, J. Lee, H.-W. Wang, R. Mejia-Rodriguez, J. H. Reibenspies, M. B. Hall and M. Y. Darensbourg, *Inorg. Chem.*, 2005, **44**, 5550–5552; (f) C. A. Boyke, J. I. Van Der Vlugt, T. B. Rauchfuss, S. R. Wilson, G. Zampella and L. De Gioia, *J. Am. Chem. Soc.*, 2005, **127**, 11010–11018; (g) J.-F. Capon, S. El Hassnaoui, F. Gloaguen, P. Schollhammer and J. Talarmin, *Organometallics*, 2005, **24**, 2020–2022.
- (a) H. Vahrenkamp, A. Geiss and G. N. Richardson, *J. Chem. Soc., Dalton Trans.*, 1997, 3643–3651; (b) J. I. Van Der Vlugt, T. B. Rauchfuss and S. R. Wilson, *Chem.–Eur. J.*, 2005, **12**, 90–98; (c) D. Chong, I. P. Georgakaki, R. Mejia-Rodriguez, J. Sanabria-Chinchilla, M. P. Soriaga and M. Y. Darensbourg, *Dalton Trans.*, 2003, 4158–4163; (d) L. Schwartz, G. Eilers, L. Eriksson, A. Gogoll, R. Lomoth and S. Ott, *Chem. Commun.*, 2006, 520–522; (e) G. Si, W.-G. Wang, H.-Y. Wang, C.-H. Tung and L.-Z. Wu, *Inorg. Chem.*, 2008, **47**, 8101–8111; (f) W.-F. Liaw, N.-H. Lee, C.-H. Chen, C.-M. Lee, G.-H. Lee and S.-M. Peng, *J. Am. Chem. Soc.*, 2000, **122**, 488–494.
- (a) L.-C. Song, J. Yan, Y.-L. Li, D.-F. Wang and Q.-M. Hu, *Inorg. Chem.*, 2009, **48**, 11376–11381; (b) D. Morvan, J.-F. Capon, F. Gloaguen, A. Le Goff, M. Marchivie, F. Michaud, P. Schollhammer, J. Talarmin, J.-J. Yaouanc, R. Pichon and N. Kervarec, *Organometallics*, 2007, **26**, 2042–2052; (c) F. Xu, C. Tard, X. Wang, S. K. Ibrahim, D. L. Hughes, W. Zhong, X. Zeng, Q. Luo, X. Liu and C. J. Pickett, *Chem. Commun.*, 2008, 606–608; (d) M.-Q. Hu, C.-B. Ma, Y.-T. Si, C.-N. Chen and Q.-T. Liu, *J. Inorg. Biochem.*, 2007, **101**, 1370–1375; (e) L. Duan, M. Wang, P. Li, Y. Na, N. Wang and L. Sun, *Dalton Trans.*, 2007, 1277–1283; (f) L. Schwartz, J. Ekström, R. Lomoth and S. Ott, *Chem. Commun.*, 2006, 4206–4208; (g) J. Windhager, M. Rudolph, S. Braeutigam, H. Goerls and W. Weigand, *Eur. J. Inorg.*

- Chem.*, 2007, 2748–2760; (h) G. A. N. Felton, B. J. Petro, R. S. Glass, D. L. Lichtenberger and D. H. Evans, *J. Am. Chem. Soc.*, 2009, **131**, 11290–11291; (i) C.-H. Chen, Y.-S. Chang, C.-Y. Yang, T.-N. Chen, C.-M. Lee and W.-F. Liaw, *Dalton Trans.*, 2004, 137–143; (j) E. J. Lyon, I. P. Georgakaki, J. H. Reibenspies and M. Y. Darensbourg, *Angew. Chem., Int. Ed.*, 1999, **38**, 3178–3180; (k) S. J. George, Z. Cui, M. Razavet and C. J. Pickett, *Chem.–Eur. J.*, 2002, **8**, 4037–4046; (l) G. Zampella, M. Bruschi, P. Fantucci, M. Razavet, C. J. Pickett and L. De Gioia, *Chem.–Eur. J.*, 2005, **11**, 509–520.
- 6 (a) M. W. W. Adams, *Biochim. Biophys. Acta*, 1990, **1020**, 115–145; (b) Y. Nicolet, A. L. De Lacey, X. Vernède, V. M. Fernandez, E. C. Hatchikian and J. C. Fontecilla-Camps, *J. Am. Chem. Soc.*, 2001, **123**, 1596–1601.
- 7 Y. Nicolet, C. Piras, P. Legrand, C. E. Hatchikian and J. C. Fontecilla-Camps, *Structure*, 1999, **7**, 13–23.
- 8 (a) M. W. W. Adams and L. E. Mortenson, *J. Biol. Chem.*, 1984, **259**, 7045–7055; (b) M. W. W. Adams, L. E. Mortenson and J.-S. Chen, *Biochim. Biophys. Acta*, 1980, **594**, 105–176.
- 9 (a) J. W. Tye, M. Y. Darensbourg and M. B. Hall, *Inorg. Chem.*, 2006, **45**, 1552–1559; (b) M. Y. Darensbourg, E. J. Lyon, X. Zhao and I. P. Georgakaki, *Proc. Natl. Acad. Sci. U. S. A.*, 2003, **100**, 3683–3688.
- 10 M. L. Singleton, R. M. Jenkins, C. L. Klemashevich and M. Y. Darensbourg, *C. R. Chim.*, 2008, **11**, 861–874.
- 11 G. Zampella, P. Fantucci and L. De Gioia, *J. Am. Chem. Soc.*, 2009, **131**, 10909–10917.
- 12 M. T. Olsen, B. E. Barton and T. B. Rauchfuss, *Inorg. Chem.*, 2009, **48**, 7507–7509.
- 13 (a) B. E. Barton, M. T. Olsen and T. B. Rauchfuss, *J. Am. Chem. Soc.*, 2008, **130**, 16834–16835; (b) B. E. Barton and T. B. Rauchfuss, *Inorg. Chem.*, 2008, **47**, 2261–2263; (c) S. Ezzaher, J.-F. Capon, F. Gloaguen, N. Kervarec, F. Y. Pétillon, R. Pichon, P. Schollhammer and J. Talarmin, *C. R. Chim.*, 2008, **11**, 906–914; (d) S. Ezzaher, J.-F. Capon, F. Gloaguen, F. Y. Pétillon, P. Schollhammer, J. Talarmin and N. Kervarec, *Inorg. Chem.*, 2009, **48**, 2–4; (e) N. Wang, M. Wang, J. Liu, K. Jin, L. Chen and L. Sun, *Inorg. Chem.*, 2009, **48**, 11551–11558; (f) N. Wang, M. Wang, T. Zhang, P. Li, J. Liu and L. Sun, *Chem. Commun.*, 2008, 5800–5802; (g) F. I. Adam, G. Hogarth, I. Richards and B. E. Sanchez, *Dalton Trans.*, 2007, 2495–2498.
- 14 F. I. Adam, G. Hogarth and I. Richards, *J. Organomet. Chem.*, 2007, **692**, 3957–3968.
- 15 A. K. Justice, G. Zampella, L. De Gioia, T. B. Rauchfuss, J. I. Van Der Vlugt and S. R. Wilson, *Inorg. Chem.*, 2007, **46**, 1655–1664.
- 16 (a) M. T. Olsen, A. K. Justice, F. Gloaguen, T. B. Rauchfuss and S. R. Wilson, *Inorg. Chem.*, 2008, **47**, 11816–11824; (b) M. T. Olsen, M. Bruschi, L. De Gioia, T. B. Rauchfuss and S. R. Wilson, *J. Am. Chem. Soc.*, 2008, **130**, 12021–12030.
- 17 Y. Nicolet, B. J. Lemon, J. C. Fontecilla-Camps and J. W. Peters, *Trends Biochem. Sci.*, 2000, **25**, 138–143.
- 18 M. Razavet, S. J. Borg, S. J. George, S. P. Best, S. A. Fairhurst and C. J. Pickett, *Chem. Commun.*, 2002, 700–701.
- 19 (a) T. Liu and M. Y. Darensbourg, *J. Am. Chem. Soc.*, 2007, **129**, 7008–7009; (b) M. L. Singleton, N. Bhuvanesh, J. H. Reibenspies and M. Y. Darensbourg, *Angew. Chem., Int. Ed.*, 2008, **47**, 9492–9495; (c) C. M. Thomas, T. Liu, M. B. Hall and M. Y. Darensbourg, *Chem. Commun.*, 2008, 1563–1565; (d) C. M. Thomas, T. Liu, M. B. Hall and M. Y. Darensbourg, *Inorg. Chem.*, 2008, **47**, 7009–7024.
- 20 (a) A. K. Justice, T. B. Rauchfuss and S. R. Wilson, *Angew. Chem., Int. Ed.*, 2007, **46**, 6152–6154; (b) A. K. Justice, M. J. Nilges, T. B. Rauchfuss, S. R. Wilson, L. De Gioia and G. Zampella, *J. Am. Chem. Soc.*, 2008, **130**, 5293–5301; (c) A. K. Justice, L. De Gioia, M. J. Nilges, T. B. Rauchfuss, S. R. Wilson and G. Zampella, *Inorg. Chem.*, 2008, **47**, 7405–7414.
- 21 J. A. De Beer, R. J. Haines, R. Greatex and N. N. Greenwood, *J. Organometal. Chem.*, 1971, **27**, C33–C35.
- 22 N. Wang, M. Wang, T. Liu, P. Li, T. Zhang, M. Y. Darensbourg and L. Sun, *Inorg. Chem.*, 2008, **47**, 6948–6955.
- 23 L.-C. Song, Z.-Y. Yang, H.-Z. Bian, Y. Liu, H.-T. Wang, X.-F. Liu and Q.-M. Hu, *Organometallics*, 2005, **24**, 6126–6135.
- 24 F. I. Adam, G. Hogarth, S. E. Kabir and I. Richards, *C. R. Chim.*, 2008, **11**, 890–905.
- 25 L.-C. Song, H.-T. Wang, J.-H. Ge, S.-Z. Mei, J. Gao, L.-X. Wang, B. Gai, L.-Q. Zhao, J. Yan and Y.-Z. Wang, *Organometallics*, 2008, **27**, 1409–1416.
- 26 L.-C. Song, C.-G. Li, J.-H. Ge, Z.-Y. Yang, H.-T. Wang, J. Zhang and Q.-M. Hu, *J. Inorg. Biochem.*, 2008, **102**, 1973–1979.
- 27 S. Ezzaher, J.-F. Capon, F. Gloaguen, F. Y. Pétillon, P. Schollhammer, J. Talarmin, R. Pichon and N. Kervarec, *Inorg. Chem.*, 2007, **46**, 3426–3428.
- 28 Y.-C. Liu, L.-K. Tu, T.-H. Yen, G.-H. Lee, S.-T. Yang and M.-H. Chiang, *Inorg. Chem.*, 2010, **49**, 6409–6420.
- 29 W. Gao, J. Ekström, J. Liu, C. Chen, L. Eriksson, L. Weng, B. Åkermark and L. Sun, *Inorg. Chem.*, 2007, **46**, 1981–1991.
- 30 S. Ezzaher, J.-F. Capon, F. Gloaguen, F. Y. Pétillon, P. Schollhammer and J. Talarmin, *Inorg. Chem.*, 2007, **46**, 9863–9872.
- 31 (a) P. Li, M. Wang, C. He, G. Li, X. Liu, C. Chen, B. Åkermark and L. Sun, *Eur. J. Inorg. Chem.*, 2005, 2506–2513; (b) W. Dong, M. Wang, T. Liu, X. Liu, K. Jin and L. Sun, *J. Inorg. Biochem.*, 2007, **101**, 506–513; (c) W.-G. Wang, H.-Y. Wang, G. Si, C.-H. Tung and L.-Z. Wu, *Dalton Trans.*, 2009, 2712–2720.
- 32 (a) X. Zhao, I. P. Georgakaki, M. L. Miller, J. C. Yarbrough and M. Y. Darensbourg, *J. Am. Chem. Soc.*, 2001, **123**, 9710–9711; (b) X. Zhao, I. P. Georgakaki, M. L. Miller, R. Mejia-Rodriguez, C.-Y. Chiang and M. Y. Darensbourg, *Inorg. Chem.*, 2002, **41**, 3917–3928; (c) R. Mejia-Rodriguez, D. Chong, J. H. Reibenspies, M. P. Soriaga and M. Y. Darensbourg, *J. Am. Chem. Soc.*, 2004, **126**, 12004–12014; (d) G. Eilers, L. Schwartz, M. Stein, G. Zampella, L. De Gioia, S. Ott and R. Lomoth, *Chem.–Eur. J.*, 2007, **13**, 7075–7084; (e) W. Dong, M. Wang, X. Liu, K. Jin, G. Li, F. Wang and L. Sun, *Chem. Commun.*, 2006, 305–307; (f) K. Wang, M. Wang, X. Liu, K. Jin, W. Dong and L. Sun, *Dalton Trans.*, 2007, 3812–3819; (g) W. Gao, J. Sun, T. Åkermark, M. Li, L. Eriksson, L. Sun and B. Åkermark, *Chem.–Eur. J.*, 2010, **16**, 2537–2546.
- 33 (a) P. Li, M. Wang, C. He, X. Liu, K. Jin and L. Sun, *Eur. J. Inorg. Chem.*, 2007, 3718–3727; (b) E. J. Lyon, I. P. Georgakaki, J. H. Reibenspies and M. Y. Darensbourg, *J. Am. Chem. Soc.*, 2001, **123**, 3268–3278.
- 34 I. P. Georgakaki, L. M. Thomson, E. J. Lyon, M. B. Hall and M. Y. Darensbourg, *Coord. Chem. Rev.*, 2003, **238–239**, 255–266.
- 35 R. H. Crabtree and M. Lavin, *Inorg. Chem.*, 1986, **25**, 805–812.
- 36 J. D. Lawrence, H. Li, T. B. Rauchfuss, M. Bénard and M.-M. Rohmer, *Angew. Chem., Int. Ed.*, 2001, **40**, 1768–1771.
- 37 (a) S. J. Borg, T. Behrsing, S. P. Best, M. Razavet, X. Liu and C. J. Pickett, *J. Am. Chem. Soc.*, 2004, **126**, 16988–16999; (b) I. Aguirre de Carcer, A. DiPasquale, A. Rheingold L. and D. M. Heinekey, *Inorg. Chem.*, 2006, **45**, 8000–8002; (c) S. P. Best, S. J. Borg, J. M. White, M. Razavet and C. J. Pickett, *Chem. Commun.*, 2007, 4348–4350; (d) G. A. N. Felton, A. K. Vannucci, J. Chen, L. T. Lockett, N. Okumura, B. J. Petro, U. I. Zakai, D. H. Evans, R. S. Glass and D. L. Lichtenberger, *J. Am. Chem. Soc.*, 2007, **129**, 12521–12530.
- 38 A. Darchen, H. Mousser and H. Patin, *J. Chem. Soc., Chem. Commun.*, 1988, 968–970.
- 39 (a) D. E. Richardson and H. Taube, *Coord. Chem. Rev.*, 1984, **60**, 107–129; (b) C. Creutz, *Prog. Inorg. Chem.*, 1983, **30**, 1–73.
- 40 J. W. Peters, W. N. Lanzilotta, B. J. Lemon and L. C. Seefeldt, *Science*, 1998, **282**, 1853–1858.
- 41 M.-H. Chiang, Y.-C. Liu, S.-T. Yang and G.-H. Lee, *Inorg. Chem.*, 2009, **48**, 7604–7612.
- 42 *SHELXTL*, ver. 6.10; Bruker Analytical X-Ray Systems, Madison, WI, 2000.